

5 DEC. 1980

Kon. Ned. Meteor. Inst.

De Bilt

1e ex.

SOME MODEL STUDIES ON THE ICE - AGE PROBLEM

JOHANNES OERLEMANS



Kon. Ned. Meteor. Inst.

De Bilt

IV. F. 90.



SOME MODEL STUDIES ON THE ICE-AGE PROBLEM

Proefschrift

ter verkrijging van de graad van doctor in de wiskunde en natuurwetenschappen aan de Rijksuniversiteit te Utrecht, op gezag van de Rector Magnificus Prof. dr. M.A. Bouman, volgens besluit van het College van Decanen in het openbaar te verdedigen op woensdag 3 december 1980 des namiddags te 4.15 uur

551.583.3

door

JOHANNES OERLEMANS

geboren op 8 oktober 1950 te Eethen

Promotor: Prof. dr. C.J.E. Schuurmans

Koninklijk Nederlands Meteorologisch Instituut, Publicatie no. 158

De Bilt, 1980

CONTENTS

	page
VOORWOORD	1
SAMENVATTING	2
SUMMARY	6
1. INTRODUCTION	
1.1 The discovery of the ice ages	9
1.2 Observational evidence	9
1.3 The astronomical theory	12
1.4 The physical problem	13
2. A CLIMATE MODEL	
2.1 Introduction	15
2.2 Model formulation	17
2.3 Parameterization of the radiative fluxes	19
2.4 Parameterization of ice and snow cover	21
2.5 Method of solution	23
2.6 Tuning of the climate model	25
3. EXPERIMENTS WITH THE CLIMATE MODEL	
3.1 Reduction of the solar constant	29
3.2 Different coefficients for energy transport	32
3.3 More active ice sheets	34
4. THE HEIGHT - MASS BALANCE FEEDBACK OF ICE SHEETS	
4.1 Representation of the mass-balance field	36
4.2 Solution diagram for a plastic ice sheet	40
4.3 Solution diagram for a flow model	44
5. THE EVOLUTION OF THE NORTHERN HEMISPHERE ICE SHEETS	
5.1 Were the ice sheets close to equilibrium ?	48
5.2 Evolution of the one-dimensional model ice sheet	49
5.3 Simulation of the growth of the Scandinavian Ice Sheet	51
5.4 Stochastic forcing of ice sheets	54

Koninklijk Nederlands
Meteorologisch Instituut
Bibliotheek,
Postbus 201,
3730 AE DE BILT.
Nederland.

6. AN ESTIMATE OF ICE/SNOW MELT VARIATIONS	
6.1 Introduction	58
6.2 A simple model for the computation of ice/snow melt	58
6.3 Results for present-day insolation	60
6.4 Model response to varying insolation	62
6.5 Parameterization of mass-balance variations	65
7. MODEL SIMULATION OF THE PLEISTOCENE GLACIAL CYCLES	
7.1 Outline of the problem	67
7.2 Incorporation of simple bedrock dynamics	69
7.3 The effect of bedrock sinking	70
7.4 Simulation of the global ice-volume record	74
8. DISCUSSION	78
REFERENCES	
A. Articles on which this thesis is based	83
B. General references	84
CURRICULUM VITAE	88

VOORWOORD

Bijna iedereen in Nederland weet wel dat er in het verleden ijstijden zijn geweest. Eens drong het ijs op tot halverwege Nederland, en de sporen die deze gebeurtenis achterliet worden in alle aardrijkskundeboeken vermeld. Hoewel er vrij veel waarnemingsmateriaal verzameld en geïnterpreteerd is, ontbreekt een afdoende verklaring voor het optreden van de ijstijden nog steeds. We kunnen dan ook rustig spreken van het 'ijstijdenprobleem'.

Het ijstijdenprobleem heeft reeds vele onderzoekers gefascineerd en bezig gehouden. Ook ik ben er niet aan ontkomen. Dit proefschrift is hiervan het resultaat, en ik hoop dat het een steentje bij zal dragen tot de oplossing van het probleem.

Het proefschrift dat voor u ligt vormt een synthese van mijn publikaties die met het ijstijdenprobleem te maken hebben (deze publikaties, waarop het proefschrift dus gebaseerd is, staan apart vermeld bij de referenties en worden in de tekst aangegeven door rechte haken). Al te technische details zijn zo veel mogelijk weggelaten, de geïnteresseerde lezer kan ze uiteraard vinden in de originele publikaties. Ook zal men soms een edukatief tintje bespeuren. Voor de deskundigen kan de uitleg van bepaalde zaken misschien wat overbodig lijken, maar ik denk dat vele anderen er mee gebaat zijn.

Rest mij een woord van dank. Het onderzoek, dat tot dit proefschrift heeft geleid, is geheel uitgevoerd op het KNMI. De werkomstandigheden waaronder dit kon gebeuren waren optimaal, waarvoor ik het KNMI zeer erkentelijk ben.

Vele kollega's hebben bijgedragen aan het onderzoek, hetzij door nauwe samenwerking, hetzij door zinnvolle kritiek. Met name Huug van den Dool, Hans Reiff, Henk Tennekes en Theo Opsteegh ben ik dankbaar voor het geduld waarmee ze naar me hebben geluisterd, en waarmee ze mijn konklusies hebben gerelativeerd.

Bij één persoon kon ik op ieder uur van de dag aankloppen: mijn promotor Cor Schuurmans. Zijn belangstelling en kritiek is van grote waarde geweest bij het onderzoek en het tot stand komen van dit proefschrift. Hiervoor ben ik hem bijzonder dankbaar.



Utrecht, september 1980

SAMENVATTING

Op aarde zijn er altijd klimaatschommelingen geweest, maar ongeveer twee miljoen jaar geleden begonnen deze een wat heviger karakter te vertonen. Tijdens de koude periodes werden er op het noordelijk halfrond grote hoeveelheden landijs gevormd (op Antarctica was reeds een permanente ijskap aanwezig), zodat de aanduiding 'ijstijd' zeer op z'n plaats is. Ruwweg zo'n 700 ka geleden (1 ka = 1000 jaar) begon er een grote regelmaat in de klimaatschommelingen op te treden, althans getuige de analyses van diepzeekernen betreffende zuurstofisotopen en het voorkomen van verschillende soorten plankton. Dit soort analyses leveren een tijdreeks van onder andere zeewatertemperaturen en het totale ijsvolume op aarde.

De grote regelmaat bestond hieruit dat er duidelijk glaciale cycli op gingen treden, die steeds ongeveer 100 ka duurden (zie Figuur 1). Deze glaciale cycli zijn in hoge mate asymmetrisch in de tijd: de opbouw van grote ijskappen gaat langzaam (50 - 100 ka), terwijl ze binnen 15 ka verdwijnen ! Dit geldt in ieder geval voor de grote ijskappen op het noordelijk halfrond, omdat deze het leeuwendeel van de variaties in het totale ijsvolume op aarde voor hun rekening nemen.

In de laatste 150 jaar zijn er vele theorieën geponeerd die het optreden van de ijstijden zouden verklaren. Bijna al deze theorieën zijn kwalitatief van aard en eigenlijk pas sinds zo'n 10 jaar wordt er daadwerkelijk aan het ijstijdenprobleem 'gerekend'. Een theorie die al meer dan een eeuw bestaat, nu en dan in de vergetelheid raakte, maar toch steeds weer opdook, is de zogenaamde astronomische ijstijdtheorie. Met name Milankovitch heeft hieraan grote bijdragen geleverd. De astronomische ijstijdtheorie zegt dat de ijstijden in wezen veroorzaakt worden door instralingsvariaties ten gevolge van veranderingen in de baan en de stand van de aarde. Recent statistisch onderzoek (zie bijvoorbeeld Hays et al.; 1976) lijkt dit te bevestigen: energiespectra van zowel het totale ijsvolume als de baanparameters van de aarde, tonen pieken bij periodes van ongeveer 20, 40 en 100 ka. Deze pieken corresponderen respectievelijk met de precessie van de equinoxen, variaties in de stand van de aardas (ten opzichte van de ecliptica) en variaties in de excentriciteit van de aardbaan.

Het vaststellen van een statistisch verband tussen instraling en ijsvolume op aarde levert uiteraard nog geen verklaring van het optreden der ijstijden, althans niet in de ogen van een fysikus. De instralingsvariatiëes van astronomische oorsprong zijn bijzonder klein (enkele procenten) en het is lang niet duidelijk hoe zulke variatiëes kunnen leiden tot enorme klimaatschommelingen zoals de ijstijden. Er zijn vele positieve terugkoppelingen in het klimaatsysteem aan te wijzen die de gevoeligheid van het klimaat voor instralingsvariatiëes sterk kunnen vergroten. Twee belangrijke, en misschien wel de belangrijkste, zijn:

(i) ijsbedekking - albedo - temperatuur terugkoppeling,

(ii) hoogte ijskap - massabalans terugkoppeling.

Kwantitatief onderzoek naar het belang van deze mechanismen vormt de kern van dit proefschrift.

De werking van mechanisme (i) kan als volgt geschetst worden. Stel dat door een of andere oorzaak de instraling op hoge breedte wat vermindert. Dit zal tot gevolg hebben dat de temperatuur daar iets lager wordt, waardoor het ijs- en sneeuwdek zich wat naar het zuiden uit kan breiden. Dit leidt tot een verhoging van het albedo (sneeuw en ijs reflekteren zonlicht in hoge mate), een verdere vermindering van de netto instraling, en dus tot een voortgaande daling van de temperatuur. Door de afnemende uitgaande straling zal dit proces op een gegeven moment wel stoppen, maar het is duidelijk dat het albedo-effekt de gevoeligheid van het klimaat sterk kan vergroten.

Het belang van mechanisme (i) kan kwantitatief onderzocht worden met behulp van klimaatmodellen. Dit wordt al sinds enige tijd gedaan, met name aan de hand van zogenaamde energiebalans-klimaatmodellen. Deze modellen zijn gebaseerd op het behoud van energie (door stro-
mingen aangevoerde warmte + netto instraling = uitstraling); er wordt aangenomen dat er zonder meer aan het behoud van impuls en massa voldaan is. De eerste experimenten met dit soort modellen, uitgevoerd in de zestiger jaren, gaven aan dat de gemiddelde temperatuur op aarde met zo'n 5 °C zou dalen als de zonnekonstante met 1 % zou verminderen.

In recente jaren is het mogelijk geworden betere modellen te konstrueren door ze te 'ijken' met satellietwaarnemingen die inmiddels ter beschikking staan. In het eerste deel van dit proefschrift wordt zo'n model besproken. Behalve door het gebruik van de meest recente

gegevens over de stralingsbalans van het aarde-atmosfeer systeem, onderscheidt het model zich van eerdere modellen door de volgende twee verfijningen. Ten eerste worden oceanische en continentale gebieden apart behandeld, waarbij energie-uitwisseling tussen deze gebieden mogelijk is. Ten tweede wordt het effect van sneeuw- en ijsbedekking op het planetaire albedo meer in detail beschreven.

De resultaten van proeven die met dit model werden uitgevoerd (besproken in hoofdstuk 3) wijzen erop dat de eerdere schattingen van de gevoeligheid van het aardse klimaat te alarmerend waren: een 1 % daling van de zonneconstante leidt tot een temperaturodaling van slechts 1,5 °C. Deze bevinding is in overeenkomst met de algehele trend: ook andere onderzoekers zijn aan de hand van satellietmetingen tot de conclusie gekomen dat het belang van mechanisme (i), de ijs - albedo - temperatuur terugkoppeling, aanvankelijk nogal overschat is.

De bovenstaande bevinding maakt het ijstijdenprobleem er niet gemakkelijker op. Blijkbaar is mechanisme (i) niet in staat de instralingsvariaties te vertalen in de klimaatschommelingen die we willen verklaren. Dit brengt ons bij de andere genoemde terugkoppeling, die van de hoogte van een ijskap op z'n massabalans (dit is de jaarlijkse resultante van sneeuwval, afsmelting, verdamping en dergelijke processen, uitgedrukt in meters ijsdikte per jaar). Naarmate een ijskap hoger wordt, zal de massabalans toenemen. Hierdoor wordt de ijskap nog hoger, zodat de massabalans verder toeneemt. Het is duidelijk dat we hier te maken hebben met een positieve terugkoppeling. Het potentiële belang van dit mechanisme werd voor het eerst expliciet genoemd door Bodvarsson (1955), en door Weertman (1961) kwantitatief aangetoond.

In dit proefschrift wordt een uitgebreide studie van de ijskap-hoogte - massabalans terugkoppeling gemaakt met behulp van modelexperimenten. Er wordt een numeriek model van de ijskappen op het noordelijk halfrond ontwikkeld, en hiermee worden experimenten gedaan waarin het model gedreven wordt door instralingsvariaties. In eerste instantie leidt ook dit tot een teleurstellend resultaat: een ijskap die zich begint te vormen in een periode met weinig instraling groeit door tot flinke afmetingen bereikt zijn (vergelijkbaar met de ijskappen die er geweest zijn), maar verdwijnt nooit meer. Zelfs een periode met relatief veel instraling blijkt de hierboven genoemde terugkoppeling niet meer te kunnen doorbreken.

De werkelijkheid leert echter anders. Getuige Figuur 1 treedt

steeds na ongeveer 80 ka een snelle afbraak van de ijskappen op. Blijkbaar worden de ijskappen, als ze eenmaal 'volwassen' zijn, instabiel. Een proces, dat deze instabiliteit zou kunnen veroorzaken, is de bodemdaling ten gevolge van de druk van de enorme ijsmassa's. Deze bodemdaling neemt pas grote vormen aan als de ijskap een flinke dikte heeft bereikt. Het effect van de bodemdaling is dat de ijskap wat lager komt te liggen, zodat de massabalans aan het oppervlak afneemt. Met de hulp van een grotere afsmelting in een periode van veel instraling zou dit tot een totale verdwijning van de ijskap kunnen leiden.

Om dit mechanisme kwantitatief te onderzoeken is het ijskapmodel uitgebreid met een vergelijking die op een ruwe manier de reactie van de bodem op de druk van de ijsmassa beschrijft. Hierbij is verondersteld dat het systeem naar handhaving van het isostatisch evenwicht streeft. Dit gebeurt niet instantaan, maar met een zekere tijdsconstante (orde van grootte: 10 ka). De bodemdaling of -stijging loopt dus altijd wat achter bij de ontwikkeling van de ijskap.

De experimenten met dit uitgebreide model geven een verrassend en hoopvol resultaat te zien: het hierboven beschreven mechanisme blijkt inderdaad op te treden ! Bovendien blijkt dat de met het model gesimuleerde curves van het ijsvolume in karakter zeer goed overeenkomen met de 'waargenomen' curves (Figuur 1). Zowel de dominerende 100 ka-periode als ook de asymmetrische vorm van de glaciële cycli verschijnen in de modelresultaten.

Een nadere analyse leert dat dit karakter van de gesimuleerde glaciële cycli vrij ongevoelig is voor variaties in de modelparameters. De precieze fase van de cycli, dat wil zeggen het tijdstip waarop ze beginnen, is hier echter bijzonder gevoelig voor. Dit duidt erop dat we met een systeem te maken hebben dat zich stochastisch-periodiek gedraagt.

De 100 ka-periode blijkt dus in feite intern gegenereerd te worden. Instralingsvariaties zijn noodzakelijk om de groei van de ijskappen in gang te zetten, maar de lengte van de glaciële cycli wordt door de dynamika van het systeem bepaald. Dit leidt tot de konklusie dat de overeenkomst in de energiespektra van het ijsvolume en de baanparameters van de aarde, voor zover het de piek bij een periode van 100 ka betreft, op toeval berust. Een statistische studie van Kominz en Piasias (1979) ondersteunt deze konklusie: een koherentiespectrum van bovengenoemde grootheden toont geen korrelatie rond 100 ka.

SUMMARY

In our geophysical knowledge, an explanation for the quarternary glacial cycles still lacks. During the last century many theories, most of them of a qualitative nature, have been put forward, but up till now one cannot state that the physical mechanism behind the regular sequence of glacials and interglacials is known.

Progress is most likely to come from quantitative model studies of the role played by the various physical processes that have been proposed as decisive factors. This thesis summarizes the results of an attempt to use mathematical modelling in this spirit.

There is one point on which many researchers (but not all) seem to agree: the quarternary glacial cycles have been forced by insolation variations associated with slight changes in the orbital parameters of the earth. This is the well-known Milankovitch hypothesis, which has recently received support from statistical studies of the correlation between global ice volume and orbital parameters (e.g. Hays et al.; 1976). The goal of the present study is to test this hypothesis in a broad sense, i.e. to see whether the physical mechanisms we know are capable of translating very small insolation variations into large climatic variations.

Two potentially important feedback loops in the climate system are studied in detail, namely

- (i) ice cover - albedo - temperature feedback
- (ii) ice-sheet height - mass balance feedback

Mechanism (i) is well known and frequently referred to as the 'albedo feedback'. Mechanism (ii) comes from the fact that the mass balance of an ice sheet (= net annual gain of ice mass) increases with increasing surface elevation. If an ice sheet grows slightly, its mass balance will thus increase which causes a further growth, etc. The importance of this feedback loop was first explicitly mentioned by Bodvarsson (1955) and discussed in more detail by Weertman (1961).

In the first part of this work, the ice-albedo-temperature feedback is studied with an energy-balance climate model. Recent data are used to parameterize the radiative and dynamic energy fluxes, and

distinction is made between continental and oceanic regions. These regions are coupled through zonal energy fluxes. The parameterization of snow and ice cover is rather detailed; simple ice-sheet dynamics are included.

The general conclusion of the experiments carried out with this model is that the strength of the ice-albedo-temperature feedback has been overestimated. The present model predicts a 1.5°C drop in global mean temperature if the solar constant would decrease by 1%. The enhancement of climate sensitivity (to insolation variations) by the ice-albedo-temperature feedback seems to be too small to explain the glacial cycles from the Milankovitch insolation variations.

The second part of this thesis deals with mechanism (ii), the feedback between the mass balance of an ice sheet and its surface elevation. A numerical model of the Northern Hemisphere ice sheets is developed and used to study the nature of this feedback loop. Model runs in which the ice sheet is forced with 'real' insolation variations lead to a disappointing result: once an ice sheet has been initiated, it grows to a large size (≈ 2500 km in meridional direction) and does not disappear anymore. A period with high insolation is not capable to break through the height - mass balance feedback.

This finding is in conflict with the observational evidence, of course. Fig. 1 clearly shows that rapid decay of the ice sheets occurred regularly. The oxygen isotope curves suggest that the ice sheets, once they are full-grown, become unstable. A process that may create unstable behaviour is bedrock sinking. A large ice sheet has a thickness of a few kilometers and thus forms a heavy load for the earth's crust beneath it. To restore an approximate isostatic equilibrium, the bedrock will sink. Consequently, the average elevation of the ice-sheet surface will decrease and the mass balance will become smaller. Together with enhanced melting in a period of increased insolation, this process may lead to a rapid decay of the ice sheet.

To investigate the effect of bedrock sinking in a quantitative way, the ice-sheet model is extended to include a damped return to isostatic equilibrium; the order of magnitude of the time scale involved is 10 ka (1 ka = 1000 years). Experiments with this model version yield an interesting result: the mechanism sketched above appears to be effective in initiating the decay of a full-grown ice sheet. Ice-volume curves simulated with the model closely resemble

'observed' curves (Fig. 1) in character. Both the strong 100 ka periodicity and the asymmetric shape (with respect to time) of the glacial cycles appear in the model results.

Variation of the model parameters shows that the duration and shape of the glacial cycles are comparatively insensitive to changes in the model parameters, whereas the phase of the simulated ice-volume record, i.e. the points in time at which the glacial cycles start, is very sensitive to such changes. This indicates that the system behaves stochastic-periodic.

In summary, the 100 ka glacial cycle seems to be an internally generated feature. It is forced by insolation variations on a smaller time scale (mainly 20 and 40 ka), but the length and shape of the cycle are determined by the ice sheet/bedrock dynamics. This leads to the conclusion that the agreement between power spectra of the global ice volume and the orbital parameters, as far as the 100 ka peak is concerned, is an accidental fact. Statistical work of Kominz and Pisias (1979) supports this view; they found that in cross spectra of ice volume and orbital parameters no coherence is present in the vicinity of this time scale.

1. INTRODUCTION

1.1 The 'discovery' of the ice ages

About 20 000 years ago, huge ice sheets covered vast regions of the North-American and Eurasian continents. Slowly and steadily those sheets carried enormous amounts of ice mass from the cold high latitudes towards the warmer regions in the south. The ice streams carried stones and rocks far away from their origin, thus providing a lot of material for the curious people that live today. Not only the land was covered by snow and ice, the northern seas experienced a similar threat. The northern part of the Atlantic Ocean was just an enormous desert of ice.

This picture of what the earth once looked like is now generally accepted; we simply call it an ice age. One and a half century ago, however, people suggesting that a large part of Europe was once covered with ice were not taken seriously. The idea of ice masses several kilometers high was considered absurd by most scientists.

Towards the middle of the nineteenth century the general opinion changed. This was in particular due to Louis Agassiz, president of the Swiss Society for Natural Sciences, who faced a number of famous scientists with traces of extensive glaciation in the Jura. The subsequent discussion lead after some years to the general acceptance of the glacial theory, as it was called in that time. In 1852 the discovery of the Greenland Ice Sheet provided definite evidence that ice sheets with a space scale of 1000 km, as described in the glacial theory, were possible. This took away all doubt.

A fascinating description of how the ideas on the glacial theory evolved can be found in Imbrie and Imbrie (1979).

1.2 Observational evidence

We will not go through all the geological evidence of ice ages, but have a look at a small part of the material only.

May be the best source of information is formed by the deep-sea record. This record has the advantages of being continuous over a

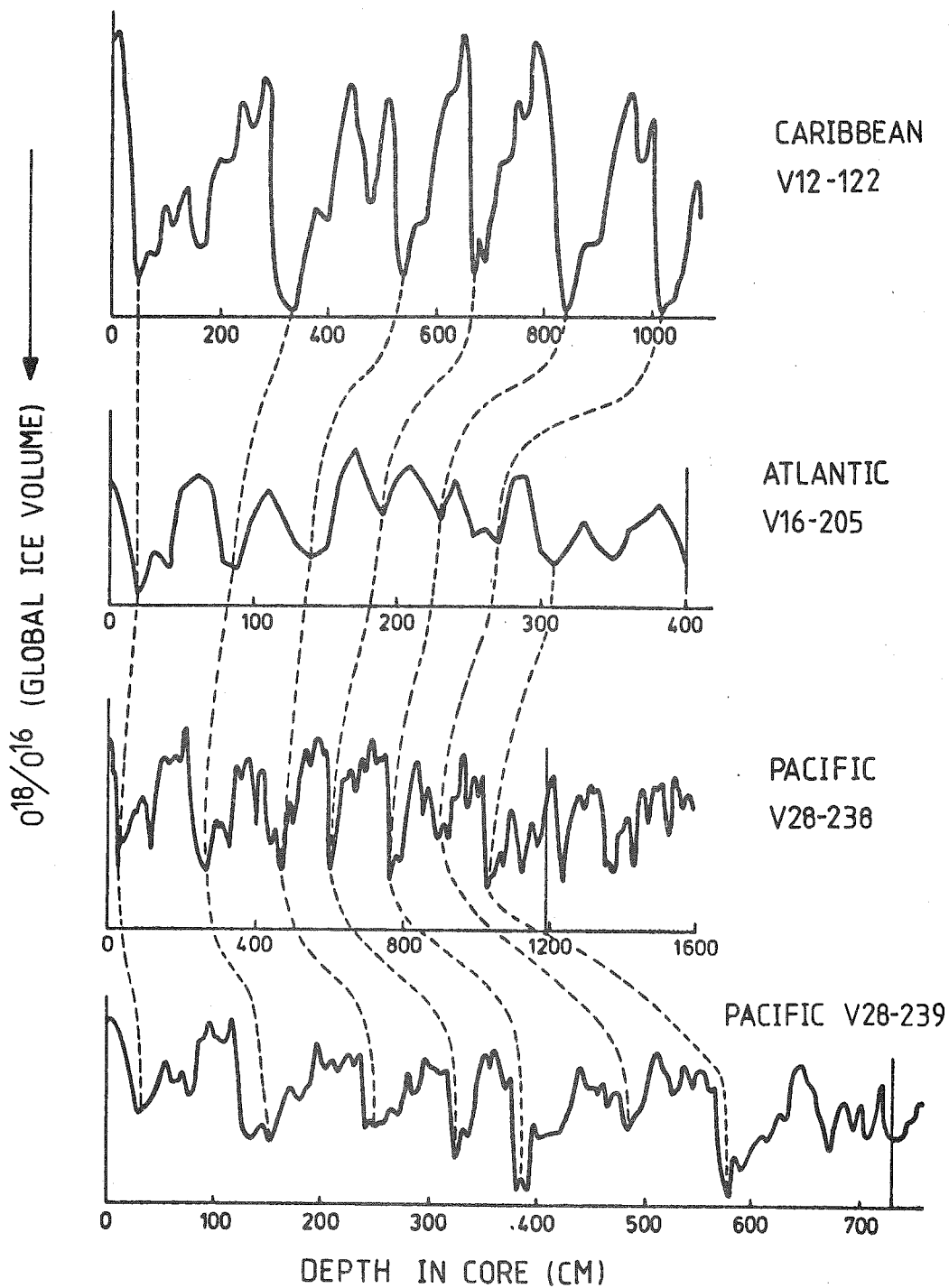


Fig. 1. A comparison of oxygen-isotope records from different deep-sea cores. Note that time runs from right to left. Sources: Imbrie et al. (1973), Shackleton and Opdyke (1973, 1976).

long period of time and of providing quantitative information. The most important quantities derived from deep-sea cores are sea-surface temperature and global ice volume. Refined statistical analysis of data on the abundance of planktonic species yields fairly reliable distributions of sea-surface temperature and sea-ice cover. Much of the pioneering work in this field was carried out by Imbrie and his collaborators, e.g. Imbrie et al. (1973).

The global ice-volume record is based on the fact that H_2O^{16} evaporates 'easier' than H_2O^{18} . So during periods with large amounts of ice on the continents the $\text{O}^{18}/\text{O}^{16}$ ratio of the oceans must also be large. Foraminefera using the sea water to build their shells thus register the ice volume. These registrations are conserved in the carbonates of their skeletons, which sink continuously to the bottom of the sea. By drawing a core out of the sea bed and analyzing its $\text{O}^{18}/\text{O}^{16}$ ratio (in the carbonates) piece by piece, a record of the global ice volume emerges.

If the $\text{O}^{18}/\text{O}^{16}$ ratio is really mainly determined by the global ice volume, and not by the water temperature at which the foramineferæ lived as was originally supposed, cores from different oceans should give essentially the same results. In Fig. 1 a number of well-known cores are compared. Along the horizontal axis the depth in the core is indicated, while the vertical axis gives the $\text{O}^{18}/\text{O}^{16}$ values (on an arbitrary scale). The thin vertical lines indicate where the Brunhes/Matyama reversal of the earth's magnetic field is located. Since we know that this reversal took place about 700 000 years ago, it provides an excellent dating point for the deep-sea records.

Although obtained from very different locations, the curves displayed in Fig. 1 show a large degree of coherency. The curves are dominated by a periodic signal, the period being roughly 100 ka (ka = kilo-annum = 1000 yrs). Locations in the cores which correspond to maximum ice volume are connected with broken lines. Except for the Atlantic core which has a very low resolution (due to a very small rate of sedimentation), we see that the 100 ka cycle is asymmetric: deglaciation proceeds much faster than glaciation. This point forms an obstacle for many ice-age theories; it will get more attention at the end of this thesis.

A remarkable effort in the reconstruction of past climates was made by the CLIMAP-project members (CLIMAP, 1976). They integrated

a large amount of geological information into a picture of what the earth's surface looked like 20 000 years ago. This picture includes ice cover, sea-surface temperature, aridity and surface albedo. It has been used as a lower boundary condition in atmospheric models in order to simulate the ice-age climate, e.g. Manabe and Hahn (1977). It also forms material to verify climate models that predict sea ice, continental ice sheets and sea-surface temperature.

1.3 The astronomical theory

The discovery of the ice ages posed an interesting theoretical problem to the natural scientist: How could the glacial cycles be explained?

The earlier theories were all simple versions of what is now known as the astronomical ice-age theory. This theory tells that ice ages are induced by insolation variations at high latitudes, which are caused by small changes in the orbital parameters of the earth. In the historical development of the astronomical theory, Adhémar, Von Humboldt, Croll and of course Milankovitch played an important role.

The astronomical theory has experienced its ups and downs, in pace with geological discoveries. Sometimes it was completely disregarded and one tried to explain the ice ages by the action of other external factors (vulcanic eruptions, interstellar dust clouds, etc.) or by internal oscillations of the climate system. The work of Van den Heuvel (1966) and Hays et al. (1976), however, has provided a statistical argument that the astronomical theory is correct: time spectra of global ice volume show peaks at periods of about 20, 40 and 100 ka, and those peaks also appear in spectra of the earth's orbital parameters (longitude of the perihelion, obliquity of the earth's axis and eccentricity of the earth's orbit, respectively). Recently, Berger (1980) has given a review of the present status of the astronomical ice-age theory.

1.4 The physical problem

Although the validity of the astronomical theory has been demonstrated in a statistical way, we are far from understanding the physical processes that are responsible for the apparent link between global ice volume and insolation variations. The central question is: 'How can small insolation variations lead to large variations in the climate?' To interpret this question in the right way, we have to be more precise about 'small' and 'large'. We may call a change in the climate large if it is larger than one would expect on the basis of a simple radiation balance in which the climate system is completely passive (no changes in albedo, etc.). Let us consider this in some more detail.

The long-term global energy balance may be written

$$\frac{1}{4} S (1 - \bar{\alpha}) = \epsilon \sigma T^4 \quad (1)$$

where S is the solar constant (1365 W/m^2), $\bar{\alpha}$ the planetary albedo (0.3), σ the Stefan-Boltzmann constant, T surface temperature and ϵ some effective emissivity of the earth-atmosphere system in the infrared region (about 0.65). Eq. (1) simply states that the absorbed solar radiation equals the net longwave radiation emitted to space. The sensitivity of this extremely simple climate model to changes in the insolation may be defined as

$$S \frac{\partial T}{\partial S} = \frac{1}{4} \left(\frac{1 - \bar{\alpha}}{4 \epsilon \sigma} \right)^{1/4} S^{1/4} = T/4 \quad (2)$$

Inserting the values of S , $\bar{\alpha}$, ϵ and σ given above, we find a value of about 70 K for this sensitivity parameter. This implies that if the solar constant decreases by 1%, a 0.7 K drop in temperature is required to restore the energy balance. If we realize that variations in the annual insolation due to varying eccentricity of the earth's orbit are within 1% of the mean insolation, it is obvious that the

Pleistocene glacial cycles (which involved global temperature changes of about 4 K) cannot be explained by this simple radiation balance model.

Numerous feedback loops exist that may increase the sensitivity of the climate (for an overview, see Pittock et al., 1978). In this thesis we consider two potentially very important feedback loops, namely, (i) the temperature-ice-albedo feedback, and (ii) the feedback between surface elevation and mass balance (= net yearly gain of ice mass) of an ice sheet.

In order to study (i), a climate model will be constructed and used in several experiments. It is completely described in terms of a yearly and vertical mean energy balance; oceanic and atmospheric dynamics only play a passive role. In spite of this, such a climate model is a useful tool in investigating the potential importance of the ice-albedo feedback.

Feedback loop (ii) requires ice-sheet modelling. Variations in global ice volume were almost entirely due to variations in the size of the North-American and Eurasian continental ice sheets (e.g. Flint, 1971). The emphasis will therefore be on those sheets. Various model studies will be discussed; they all point to the extreme importance of (ii).

2. A CLIMATE MODEL

2.1 Introduction

The earth and its atmosphere exchange energy with space in very large amounts (compared to the thermal inertia of the active part of the climate system), while the exchange of mass and momentum is small. If one is interested in the global climate, a model of the earth-atmosphere system based on an energy balance only seems to be a good start. Budyko (1969) and Sellers (1969) first investigated the sensitivity of the earth's climate with a so-called energy-balance climate model. Since that time energy-balance climate models have got much attention. Notable contributions are those by Held and Suarez (1974), North (1975), Gal-Chen and Schneider (1976) and Lian and Cess (1977).

The first results obtained with energy-balance climate models were alarming: the models of Budyko and Sellers predicted a totally glaciated earth if the solar constant would drop by about 2 %, a consequence of the strong temperature-ice-albedo feedback in their models. Gradually the picture has changed and things seem less dramatic than suggested by the earlier models.

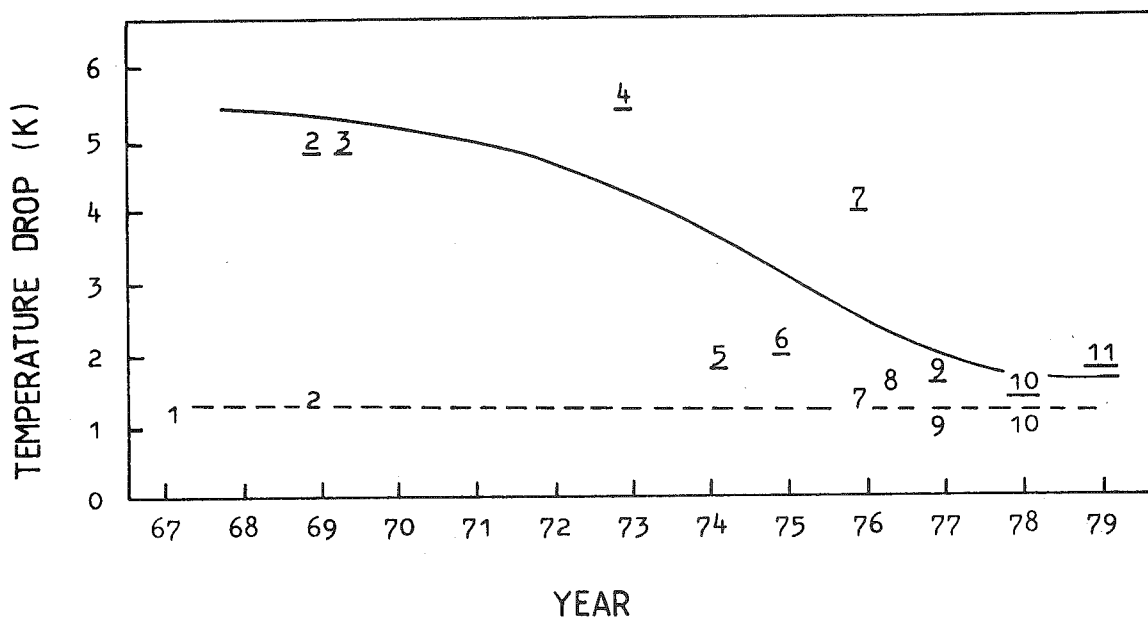
An overview of how thoughts about global climate sensitivity have evolved is presented in Fig. 2. It shows estimates of the drop in global mean surface temperature to be expected if the solar constant would decrease by 1 %. Underlined figures refer to model experiments in which ice-albedo feedback is included. With the exception of Manabe and Wetherald (1967, radiative-convective model) and Wetherald and Manabe (1975, general circulation model), all studies were carried out with energy-balance climate models.

In Fig. 2, the distance between the solid line (including ice-albedo feedback) and the dashed line (no ice-albedo feedback) measures the importance of the ice-albedo feedback in enhancing climate sensitivity. It is evident that the ice-albedo feedback has been overestimated considerably. The increasing stream of satellite data on the radiation balance of the earth has led to the conclusion that ice-albedo feedback amplifies the sensitivity of the climate by 30 to 50 %.

In this chapter a climate model will be designed by making use

Fig. 2. Drop in global mean temperature for a 1 % decrease in the solar constant, according to several authors. Bars indicate inclusion of ice-albedo feedback.

References: 1 = Manabe and Wetherald (1967), 2 = Budyko (1969), 3 = Sellers (1969), 4 = Schneider and Gal-Chen (1973), 5 = Sellers (1974), 6 = Wetherald and Manabe (1975), 7 = Gal-Chen and Schneider (1976), 8 = Cess (1976), 9 = Lian and Cess (1977), 10 = Oerlemans and Van den Dool (ref. [1]), 11 = Coakley (1979). The figure does not pretend to be complete, it is ment to show the general tendency.



of most recent data to parameterize the components of the energy budget. Separate treatment of the energy budget over continental and oceanic regions makes it possible to investigate the role of zonal asymmetry in climatic change. In chapter 3 we will use this climate model to re-investigate the ice-albedo feedback, and also to assess the potential importance of varying energy transports by the oceanic and atmospheric circulation.

2.2 Model formulation

Consider a column extending from the 'top' of the atmosphere through the ocean downwards to a depth in the earth's crust where the influence of the radiation coming from space is negligible. Fig. 3 shows a south-north cross section of such a column. All fluxes are zonally averaged. In case of equilibrium, the following energy balance should hold

$$\text{div (atm. + oceanic heat flux)} + Q(1-\alpha) = I \quad (3)$$

It states that the divergence of the northward heat flux plus the amount of absorbed solar radiation $Q(1-\alpha)$ (Q is insolation at top of atmosphere, α the planetary albedo) equals the outgoing longwave (infrared) radiation I . If all terms in eq. (3) can be expressed in surface temperature, this temperature can then be solved for any prescribed value of Q , at any latitude. Before doing so, we make the model slightly more realistic.

Dividing each latitude circle into an oceanic and a continental part, and formulating separate energy balances for these parts adds internal freedom to the model: zonal asymmetry, i.e. temperature differences between land and ocean, may be created.

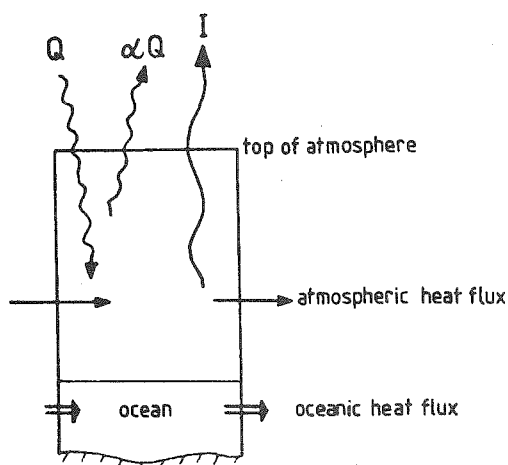


Fig. 3. Components of the energy balance. Latitude increases from left to right, and the fluxes are averaged along latitude circles.

Zonal asymmetry will be damped by zonal heat fluxes, so it is necessary to include such fluxes in the climate model. Fig. 4 illustrates the resulting model configuration. Continental and oceanic annual sea-level temperatures are denoted by T and θ respectively, and energy fluxes are proportional to the corresponding temperature gradients. The model equations are

$$\text{div} (D_o \text{ grad } \theta) + Q(1-\alpha_o) = I_o + D(\theta-T)/(1-\Delta), \quad (4)$$

$$\text{div} (D_c \text{ grad } T) + Q(1-\alpha_c) = I_c + D(T-\theta)/\Delta. \quad (5)$$

The subscripts o and c refer to oceanic and continental part; Δ is the fraction of land along a latitude circle, it is taken constant with latitude to prevent meridional energy fluxes from contributing directly to the ocean-to-land (i.e. zonal) energy flux. The latter is represented by the last terms in eqs. (4) and (5). It should be noted that eq. (4) applies to the oceanic part, not to the ocean; D_o reflects the total 'capability' of transporting energy polewards, thus including the atmospheric contribution.

It is possible to derive from observational data (Oort and Vonder Haar, 1976; Oort, 1980) an estimate of D_c/D_o . It appears that at low and middle latitudes D_c/D_o has a value of 0.45 to 0.6, while at high latitudes the ocean contributes very little and the value of D_c/D_o is closer to 1 (ref. [2]). The latter is mainly due to the

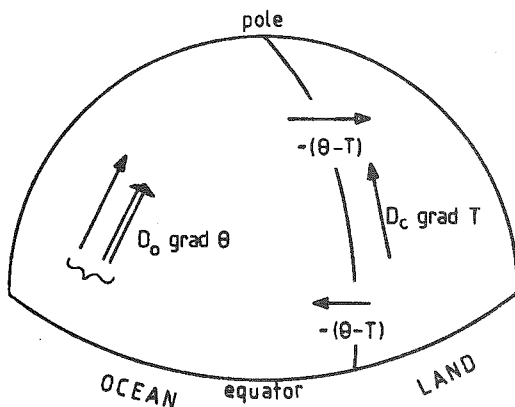


Fig. 4. Configuration of the climate model. Heat transports by ocean and atmosphere are set proportional to the corresponding sea-level temperature gradients.

presence of sea ice. In the climate model we will use a constant (latitude independent) value of D_c/D_o , except when sea ice is present in which case D_c/D_o is set to 1.

The coefficient for the zonal heat flux is written:

$$D(\varphi) = kV^*(\varphi)/\cos \varphi, \quad (6)$$

where φ is geographical latitude, k some constant and $V^*(\varphi)$ a characteristic zonal wind speed at the 850 mbar level (taken from Oort and Rasmusson, 1971). The factor $1/\cos \varphi$ accounts for the poleward decrease of the ocean-continent distance.

It is important to note that the representation of the heat fluxes involves three constants: D_c , D_c/D_o and k . Those constants can be used to tune the model, i.e. to obtain a best model simulation of the present sea-level temperature distribution. D_c determines the pole-equator temperature difference, while k and D_c/D_o determine the zonal asymmetry $\theta-T$.

2.3 Parameterization of the radiative fluxes

The outgoing longwave radiation is expressed in terms of surface temperature and cloudiness according to

$$I_o = A_o + B\theta_s + CN_o; \quad I_c = A_c + BT_s + CN_c. \quad (7)$$

A_o , A_c , B and C are constants, and N_o , N_c represent cloudiness which is a function of latitude. The subscript s refers to surface. This type of linear regression fits very well the observed satellite data (Van den Dool, 1980). The value of B ($= \partial I_c / \partial T_s = \partial I_o / \partial \theta$) strongly effects the stability of the model climate (ref. [1]). It should account for the temperature - water vapour feedback in the atmosphere. With regard to the discussion in section 1.4, this means that ϵ becomes temperature dependent: it decreases with temperature.

At present, the best way to obtain values of the constants in eq. (7) is to employ zonal climatology, i.e. to relate observed values of $I(\varphi)$ to observed values of temperature and cloudiness. This procedure automatically includes the water vapour feedback, but some caution is needed (Cess, 1976; Coakley and Wielicki, 1979). We use values of A, B and C presented by Van den Dool (1980); they are based on satellite data compiled by Ellis and Vonder Haar (1976) and a cloud climatology of Berliand and Strokina (1975). In a later stage A_o and A_c will be varied slightly to fit the model climate to the observed one in an optimum way. $N_o(\varphi)$ and $N_c(\varphi)$ are prescribed functions of latitude according to Berliand and Strokina (1975).

The amount of absorbed shortwave (solar) radiation is affected by the climate system through the planetary albedo $\alpha(\varphi)$. This albedo is first divided into contributions from overcast and clear-sky regions (N represents N_o or N_c):

$$\alpha = \alpha_{\text{clear}}(1-N) + \alpha_{\text{cloud}}N \quad , \quad (8)$$

where α_{clear} is the clear-sky albedo and α_{cloud} the cloud albedo. The dependence of cloud albedo on the zenith angle of the sun is taken into account. Values of α_{cloud} can be derived from the same data used in parameterizing the infrared radiation (Van den Dool, 1980).

The clear-sky albedo deserves special attention, because it should reflect the effect of varying surface conditions. Most important is whether ice or snow cover is present. If so, the clear-sky albedo is considerably higher than in case of bare land or open sea. How ice and snow cover can be expressed in terms of temperature is discussed in the next section.

Table I provides a list of constants used in the formulation of the radiative fluxes. Quantities depending on latitude are not given here; they may be found in Van den Dool (1980). To give some idea, cloud albedo runs from about 0.35 at the equator to about 0.65 at the poles.

Table I. Constants used in the parameterization of the radiative fluxes. The values are mainly based on satellite data (for longwave radiation: Ellis and VonderHaar, 1976; for clear-sky albedos: Raschke et al. (1973)).

<u>Longwave radiation</u>			
A_o	231		W/m^2
A_c	225		W/m^2
B	2.04		$W/(m^2 K)$
C	-38.8		W/m^2
<u>Clear-sky albedo over</u>			
open sea	0.13		
bare land	0.22		
ice cover	0.56		
snow cover	0.61		

2.4 Parameterization of ice and snow cover

Sea ice and snow cover are supposed to be directly related to annual temperature. The representations employed here are shown in Fig. 5. They are derived from present-day climatology; see ref. [1] for more details.

In the 'classical' energy-balance climate model, no difference exists between ice cover over land and sea. The equatorward tip of the ice cover coincides with some isotherm. Often the $-10^\circ C$ isotherm is used. In the present model we distinguish between sea ice and continental ice. There is a very good reason to do so.

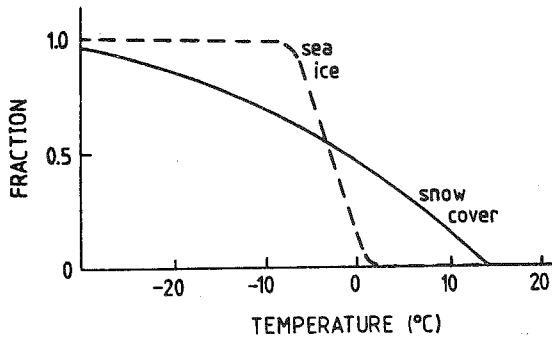


Fig. 5. Representation of sea ice and snow cover in the model. In the case of sea ice, fraction refers to the oceanic part along a latitude circle; in the case of snow cover, to land and frozen ocean.

Since large continental ice sheets may be a few kilometers thick, gravitational forces may become so large that enormous amounts of ice mass flow southwards into regions with high insolation.

Fig. 6 shows a typical Northern Hemisphere situation during glacial conditions. In this meridional cross section the northern edge of the continent is located at a latitude of about 70°N . The polar sea acts as an infinite sink for ice. In a first approximation, the mass balance of the ice sheet (net yearly gain of ice at the surface in m/yr , denoted by G) increases linearly with latitude. No ice flows through the centre of the sheet, because the horizontal pressure gradient is zero here. Consequently, in a steady state the mean mass balance over the northern half of the sheet equals the production of ice bergs at the northern edge. The steady-state size L of the ice sheet is found by equating the average mass balance of the

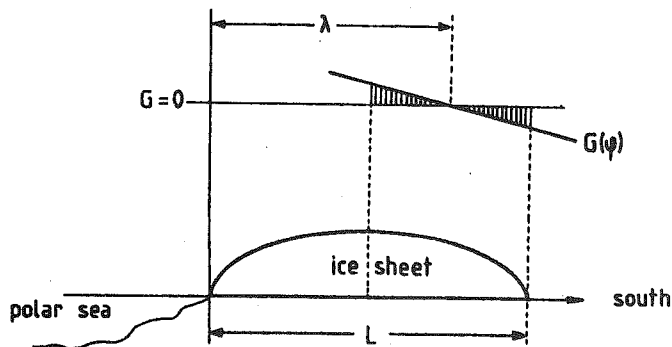


Fig. 6. Meridional cross section through a Northern Hemisphere continental ice sheet of size L . Mass balance conditions are shown in the upper part.

southern half to zero. We then find

$$L = \frac{4}{3} \lambda, \quad (9)$$

where λ is the distance between the polar sea and the point at which $G = 0$. We now assume that this point coincides with some surface temperature T^* . A value of about -12°C for T^* seems to be in agreement with present-day conditions. So continental ice sheets start to grow as soon as the annual surface temperature drops below -12°C .

The present way of including continental ice sheets implies that the larger the ice sheet, the higher the temperature at the southern edge. For the classical ice-line concept mentioned earlier, the temperature at the southern edge is constant. For a more detailed discussion of this topic, see ref. [3].

At this point it should be mentioned that the height of the ice sheet and the consequent decrease of surface temperature has been ignored. We return to this later.

2.5 Method of solution

Eqs. (4) and (5) are solved by an iterative method. This is necessary because the temperature-ice-albedo feedback and the effect of sea ice on the poleward heat flux make the system nonlinear in T and θ .

The solution is computed on a grid with 18 grid points between equator and pole, defined by

$$\varphi_i = 2.5 + 5(i-1)^\circ\text{N}, \text{ with } i = 1, \dots, 18. \quad (10)$$

Only the Northern Hemisphere is considered. Imposed boundary conditions are that there be no meridional energy flux across the equator and pole. This is accomplished by setting $\text{grad } T = 0$ and $\text{grad } \theta = 0$ at these locations. If the differential operators in eqs. (4) and (5) are

replaced by central differences, these equations take the form

$$\begin{aligned} A\vec{T} &= \vec{f}(\vec{\theta}, \vec{T}) \\ D\vec{\theta} &= \vec{g}(\vec{\theta}, \vec{T}) \end{aligned} \quad (11)$$

A and D are matrices representing the flux divergence operator and the coefficient for the infrared damping (which is $-BT$, $-B\theta$ respectively). \vec{T} and $\vec{\theta}$ are vectors with elements $T(\varphi_i)$ and $\theta(\varphi_i)$, and \vec{f} and \vec{g} denote the remaining components of the energy balances (absorbed solar radiation, constant part of I, zonal heat fluxes which make \vec{f} and \vec{g} a function of both $\vec{\theta}$ and \vec{T}).

A and D are band matrices with three diagonals and can easily be inverted by some standard numerical method. The following scheme appeared to work satisfactorily in obtaining the equilibrium solutions of the climate model:

$$\begin{aligned} \vec{T}_{j+1} &= \mu A^{-1} \vec{f}(\vec{\theta}_j, \vec{T}_j) + \nu \vec{T}_j, \\ \vec{\theta}_{j+1} &= \mu D^{-1} \vec{g}(\vec{\theta}_j, \vec{T}_j) + \nu \vec{\theta}_j, \end{aligned} \quad (12)$$

$$\text{with } \mu + \nu = 1.$$

The index j indicates the number of the iteration. The constants μ and ν are needed to damp oscillations that sometimes occur in the iterative process. For most experiments, $\mu = 0.3$ and $\nu = 0.7$ performed quite well. Various minor modifications of scheme (12) were used during the experiments with the climate model; they will not be described here.

Finally, it is important to realize that scheme (12) only gives stable equilibrium solutions; unstable solutions will not show up. In practice this is not a serious problem because unstable solutions will not appear in nature.

2.6 Tuning of the climate model

If we would know accurately from observations or basic physical considerations all the constants used in the formulation of the heat fluxes and the radiative fluxes, and if the climate model would be based on the right physics, the present climate should perfectly show up as a solution of eqs. (4) and (5). The situation is less fortunate, however. Slight changes in some model constants may yield very different climates. The best procedure seems to be to tune the model to present-day conditions, i.e. to adjust the model constants in such a way that the present temperature distribution, which is rather well known, is simulated best.

The fact that the number of empirical constants is rather large implies that the climate model does not have much internal freedom. Once the constants are determined, the model behaviour for different forcing is restricted to a rather narrow band of possibilities. For example, the fact that cloudiness is not allowed to vary puts rather strong limits to the planetary albedo. In interpreting the forthcoming results, this should be remembered.

Table II gives an overview of the constants involved. There are essentially four quantities that can be used to tune the model: hemispheric mean temperature, hemispheric mean zonal asymmetry, meridional gradient of the zonal mean temperature, and zonal asymmetry. Note that the last two quantities determine the difference in the meridional temperature gradients over the oceanic and continental parts.

The experiments carried out to tune the model are described in ref.[2]. Here we only discuss the result. The best simulation of the present climate that can be obtained with the model has a rms-error of 1.07 K (with respect to data given by Oort (1980), computed over 36 points: T_i and θ_i , $i=1, \dots, 18$). The corresponding model constants are: $A_o = 231$, $A_c = 225 \text{ W/m}^2$; $D_c = 0.48 \text{ W/(m}^2 \text{ K)}$; $k = 0.05 \text{ W s/(m}^3 \text{ K)}$; $D_c/D_o = 0.6$. In this simulation the fraction of land along a latitude circle was 0.4 and the surface elevation of the land was 300 m. The latter means that over the continent the surface temperature, which is used in the computation of the radiative fluxes, is always about 2 K lower than the sea-level temperature.

Table II. An overview of the constants introduced in the climate model by the parameterization of the radiative fluxes and heat transports.

Fixed constants:

cloudiness (Van den Dool, 1980)
 cloud albedo (Van den Dool, 1980)
 clear-sky albedos (Table I)
 infrared damping (Table I)
 fraction of land (0.4)
 surface elevation of land (300 m)
 ice/snow cover (Fig. 5)

Tuning constants:

$A_c + A_o$ hemispheric mean temperature
 $A_c - A_o$ hemispheric mean zonal asymmetry
 D_c meridional gradient of zonal mean temperature
 $\left. \begin{array}{l} D_c/D_o \\ k \end{array} \right\}$ zonal asymmetry

Fig. 7 shows the zonal mean temperature, defined as $(1-\Delta)\Theta + \Delta T$, as a function of latitude. Crosses indicate observed values. Apparently the model simulation is excellent except at very low and very high latitudes. At those locations the simulated climate is too warm. The probably reason for this is that in the equatorial and polar regions the sea-level temperature is not representative for the whole column due to the dominance of boundary layer processes, and that the redistribution of heat does not obey a diffusion-type law at these latitudes. The latter has been discussed

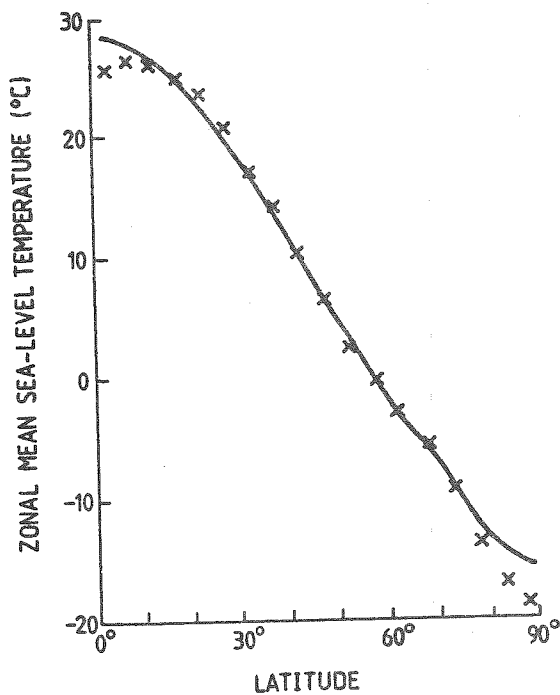


Fig. 7. Computed distribution of zonal mean temperature (solid line). The crosses denote observed values (Oort, 1980).

thoroughly by Lindzen and Farrell (1977).

Fig. 8 displays the computed zonal asymmetry. The observed distribution of θ -T is reasonably well simulated by the model. The picture is dominated by a peak around 65°N. It is caused by two processes, namely, the large amount of heat carried northward by the oceans at low and middle latitudes and the difference in surface albedo between ocean and continent at the middle to high latitudes. The observed peak is much higher than the simulated one, but this may be attributed completely to the schematic representation of the ocean-continent configuration in the model. The observed peak reflects the narrow but very warm Norwegian Sea, which is badly resolved by the climate model.

The overall impression from Figs. 7 and 8 is that the present climate is simulated reasonably well. From a climate model with very schematic geometry and in which neither large scale ocean/atmosphere dynamics nor boundary layer processes are treated explicitly, one cannot expect more.

In the following chapter a number of experiments carried out with the above-described basic version of the model will be discussed.

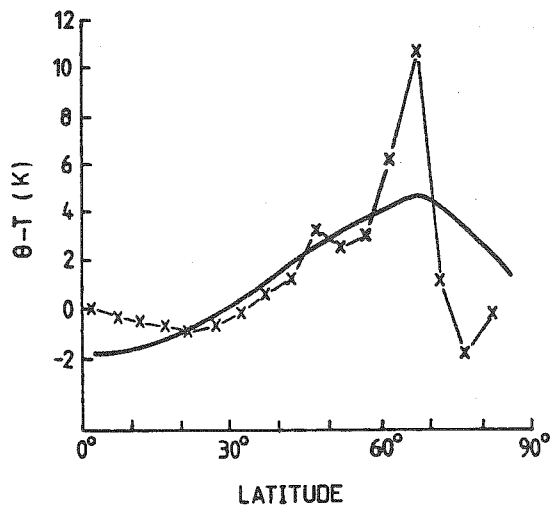


Fig. 8. Zonal asymmetry, defined by $\theta - T$, as a function of latitude. The solid line represents the model simulation and crosses indicate observed values (computed from Oort, 1980).

3. EXPERIMENTS WITH THE CLIMATE MODEL

3.1 Reduction of the solar constant

The most straightforward way of investigating the sensitivity of the model climate is to decrease the solar constant S , which means that at each latitude the insolation is reduced by the same factor. A drop of the solar constant does not necessarily stem from a decreased solar luminosity, but may also reflect the effect of an increased dust concentration above the troposphere. Such a dust shield may for example occur in periods of pronounced volcanic activity. Variations in the eccentricity of the earth's orbit may also be translated into variations of the solar constant.

Fig. 9 shows how much the model climate cools if S is decreased by 2%. The temperature drop is largest at high latitudes, which is due to vanishing oceanic heat transports if sea ice is present. At moderate latitudes the temperature drop over land is larger than over sea, a consequence of the stronger albedo feedback over land for temperatures in the 0-15 °C range. In addition to this, at those latitudes cloudiness over land is about 20% less than over sea, which makes the albedo feedback more effective.

A 2% decrease of S is quite large, and it is generally believed that larger drops did not occur during the last million years. To show that even much larger drops would be needed to create Northern Hemisphere ice sheets of ice-age size, Fig. 10 displays some results of experiments with larger reductions of S .

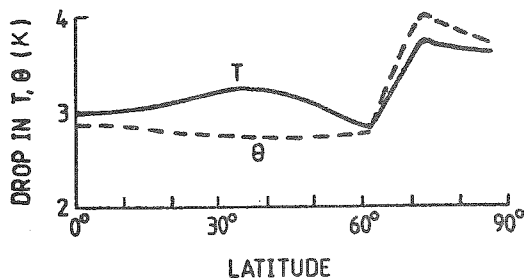


Fig. 9. Temperature drop in oceanic and continental regions for a 2% decrease of the solar constant S .

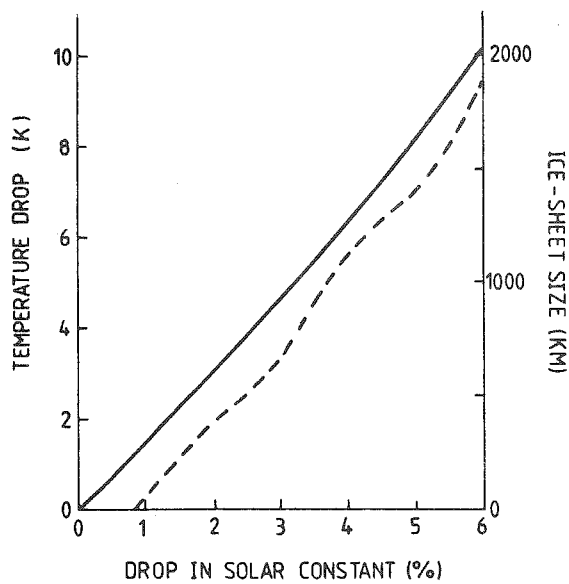


Fig. 10. Drop in hemispheric mean temperature (solid line) and ice-sheet size (broken line) as a function of the solar constant S .

Apparently, a drop of at least 6 % would be required to establish a full size ice sheet. In that case the hemispheric mean temperature would be 10 K below its present value, which is more than twice the value indicated by proxy data (CLIMAP, 1976).

An interesting question is whether zonal asymmetry is sensitive to variations in S . Values of $\theta - T$ at 62°N and 42°N are shown in Fig. 11. At high latitudes zonal asymmetry hardly changes if S decreases. At middle latitudes, however, zonal asymmetry changes considerably. This is caused by differences in the strength of the albedo feedback over land and ocean. Nevertheless, the enhancement of zonal asymmetry is still too small to create large continental ice sheets for a small reduction of the solar constant.

The experiments discussed in this section all indicate that the albedo feedback does not amplify the sensitivity of the climate so much that variations in S of about 1 % may explain the occurrence of glacial cycles. This result is largely due to the presence of clouds. In particular at high latitudes cloudiness is large and since it is fixed in the model, the albedo feedback is strongly limited.

A more detailed discussion on this topic is given by Van den Dool (1980).

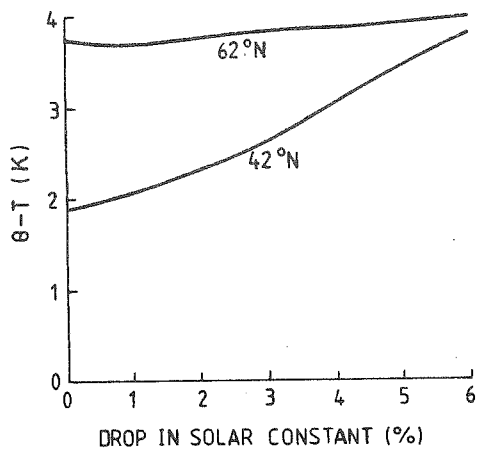


Fig. 11. Zonal asymmetry at two latitudes as a function of the solar constant S.

To assess the importance of the albedo feedback, an experiment in which the model is forced by a continental ice sheet of fixed size is also useful. Table III lists some results of such an experiment. In both cases the present solar constant was used! We see that even for $L = 3000$ km temperature drops are rather small. The last column shows that the effect of continental ice sheets on the hemispheric albedo is not very large.

Table III. Model response for two prescribed values of the continental ice-sheet size L . An overbar denotes a hemispheric mean value; subscripts refer to latitude. All values represent deviations from present. Temperatures are in K.

L (km)	$\bar{\theta}$	\bar{T}	θ_{62}	T_{62}	$\bar{\alpha}$
1500	-0.17	-0.30	-0.25	-0.71	+0.0012
3000	-0.77	-1.84	-1.22	-2.64	+0.0081

With regard to hemispheric mean temperature (T_h) and hemispheric albedo ($\bar{\alpha}$), the strength of the albedo feedback due to changes in ice-sheet size is (estimated from Table III)

$$\left. \frac{\partial T_h}{\partial \bar{\alpha}} \right|_{S_0} \approx 0.006 \text{ K} \quad (13)$$

A more general estimate of the strength of the albedo feedback can be obtained directly from eq. (1) by differentiating the expression for T to $\bar{\alpha}$ and inserting the values of the constants given in section 1.4. This yields a value of 0.010 K. The difference between these estimates of the hemispheric albedo feedback stems from the fact that in the model experiments the largest albedo changes occur at latitudes with relatively small insolation, while in using eq. (1) one implicitly assumes that the change in albedo is uniform over the hemisphere.

3.2 Different coefficients for energy transport

Internally or externally forced changes in the oceanic and atmospheric circulation may strongly affect the capability of the climate system to redistribute energy. With the present model the potential importance of such changes can be investigated by carrying out experiments with different values of D_c , D_o and k . Such experiments may also give valuable insight in how the present temperature distribution is established.

In a first experiment zonal heat fluxes were set to zero ($k = 0$),

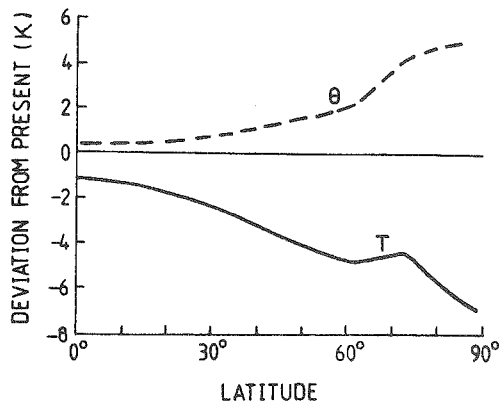


Fig. 12. Change in temperature if zonal heat fluxes would cease. The oceanic part warms while the continental part cools.

which means that the energy balances over land and ocean are completely decoupled. Such a situation simulates an upper bound for the possible effect of strong meridional circulation patterns in the atmosphere. Fig. 12 shows the resulting model climate, in terms of temperature deviations from present. It is obvious that the ocean-continent contrast sharpens: oceanic regions become warmer, continental regions colder. This effect increases with latitude.

Next, we consider the question of what would happen if the oceans stops transporting energy. To simulate this situation D_o is set equal to D_c . The result of such a model run is shown in Fig. 13. The change in temperature is only given for the oceanic part, because the change for the continental part is similar (difference smaller than 0.7 K everywhere). The curve illustrates in a very clear way how important the oceanic heat flux is in establishing the present climate. Without this flux the meridional temperature gradient would be much larger, thus allowing the continental ice sheets to have a size of 1270 km. The corresponding decrease of the hemispheric temperature would be 1.4 K.

The foregoing experiments give some indications on the potential importance of changing circulation patterns in climatic change on the large scale. More extensive experiments with other values of D_c and D_o are described in ref. [2].

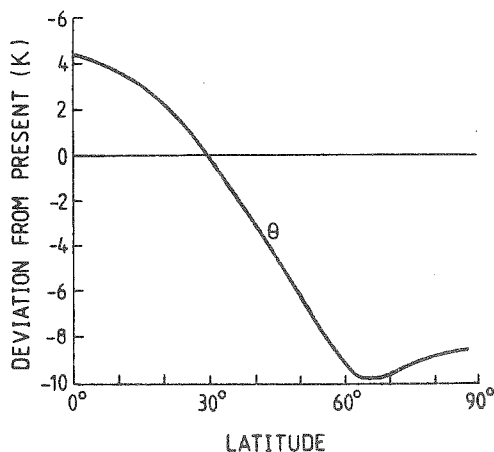


Fig. 13. Change in oceanic temperature if the oceans would not carry energy anymore. The result for the continental part is similar.

3.3 More active ice sheets

In the preceding experiments the height of the ice sheet has not been taken into account. It is obvious, however, that the surface temperature over the ice sheet will decrease if the sheet becomes higher. This makes the mass balance of the sheet larger, so it will continue to grow. This feedback loop, the height-mass balance feedback, may be very important. Bodvarsson (1955) was among the first to emphasize this point.

The way in which a Northern Hemisphere ice sheet is incorporated in the climate model is in fact not sophisticated enough to assess the importance of the height-mass balance feedback. Nevertheless, to get an impression of what might happen an experiment was carried out in which the surface temperature in the continental part (T_s) was computed with

$$T_s = T - (H+300)\Gamma . \quad (14)$$

In eq. (14), H is the thickness of the ice sheet and Γ some lapse rate (here, 0.0065 K/m). H is obtained from the assumption that the ice flows as a perfectly plastic substance. In this case the ice-sheet profile is given by (e.g. Paterson, 1969)

$$H(x) = \sigma \left[\frac{1}{2} L - \left| x - \frac{1}{2} L \right| \right]^{1/2} . \quad (15)$$

L is the size of the sheet and x the distance to the polar sea along a meridian (see Fig. 6). The constant σ determines the height-to-width ratio of the sheet and follows from the appropriate value of the yield stress (this value is larger if the ice is colder). In the experiment discussed below $\sigma = 3.5 \text{ m}^{1/2}$. For example, if an ice sheet has a size of 2000 km, the corresponding value of its height at the centre will be 3500 m. This value of σ is rather large (it may apply to a cold ice sheet like the Antarctic one), so if the height-mass balance feedback is important, it will be brought to light.

The experiment of varying the solar constant S was now repeated with inclusion of eqs. (14) and (15). Fig. 14 displays the results

in terms of hemispheric mean temperature (T_h) and ice-sheet size. The results are very different from those of Fig. 10. The model climate shows hysteresis, apparently due to the inclusion of the height-mass balance feedback. For a drop in S of more than 2.7 % the only solution is a climate in which the ice sheet reaches the equator. On the other hand, if the drop is less than 2.2 % only a small ice sheet is possible. In between, the climate model produces two stable equilibrium states, the difference in T_h between those states being about 7 K.

Fig. 14 should not be taken too literally because the ice sheet has been treated in a very schematic way. Other values of σ and Γ change the picture to some extent, but the hysteresis always occurs. We may therefore conclude that the height-mass balance feedback creates an impressive nonlinearity in the model, which should be investigated carefully. We turn to this in the next chapter.

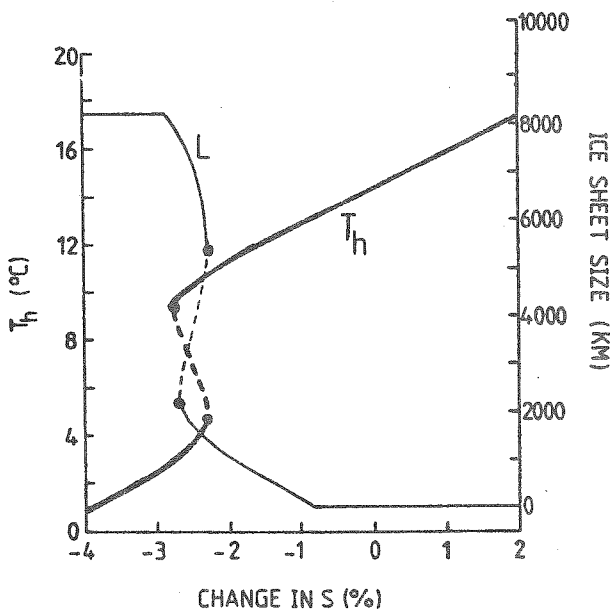


Fig. 14. Solution diagram of the climate model with regard to the solar constant S . Heavy line: hemispheric mean temperature T_h ; thin line: ice-sheet size L . The broken lines represent unstable equilibrium solutions; dots are critical points.

4. THE HEIGHT-MASS BALANCE FEEDBACK OF ICE SHEETS

4.1 Representation of the mass-balance field

In studying the effect of the height-mass balance feedback, one has to know how the annual mass balance G depends on surface elevation and geographical location. Measurements on present day glaciers and ice sheets can be used, but it is very unlikely that the resulting parameterization of G would be representative for the conditions that prevailed over the Laurentide (North-America) and Eurasian Ice Sheet. Valley glaciers at moderate latitudes are subject to typical valley climates and are in most cases of small size, which implies that they effect the climate much less than large ice sheets. However, the large ice sheets that exist today (Antarctic and Greenland Ice Sheet) are located at high latitudes and therefore subject to a cold climate - probably colder than that over the Laurentide and Eurasian Ice Sheet. It is due to these difficulties that some ambiguity cannot be avoided in the parameterization of G .

About one point we are certain: G increases with both height and latitude. Measurements also show that G decreases with increasing distance to open sea (e.g. Chorlton and Lister, 1971). This is mainly due to differences in precipitation amount. Except for the experiment in which the growth of the Eurasian Ice Sheet is simulated (chapter 6), we will ignore this 'continentality effect'.

A frequently employed formulation of G is of the type

$$G(x,h) = \psi(h-E) ; \quad E(x) = (x-P)\chi . \quad (16)$$

It states that the mass balance is a function of height with respect to the equilibrium-line altitude E , defined as the altitude at which $G = 0$. E is assumed to increase linearly with the distance x to the polar sea (see Fig. 15), so the slope of the equilibrium line (χ) is positive. P is the position of the point where the equilibrium line intersects sea level, it is called the 'climate point' because it will serve as indicator for the prevailing climatic conditions.

Fig. 15 gives an example of a mass-balance field. It shows lines of equal mass balance in a height-latitude cross section. For present conditions $P < 0$, i.e. the climate point is located in the polar sea. In model experiments climatic variations may be simulated by shifting P north- and southward. As soon as P comes on the continent, an ice sheet forms.

The function ψ can reasonably well be approximated by a parabolic curve (see Fig. 16), together with the condition that the mass balance is constant (G_c) for $h > h_c - E$. So we write

$$G = a(h-E) + b(h-E)^2 \quad \text{if } h < h_c - E ,$$

$$G = G_c \quad \text{if } h \geq h_c - E .$$

The constants a , b , h_c and G_c are chosen in such a way that at the top of the parabola $G=G_c$ and $h=h_c - E$.

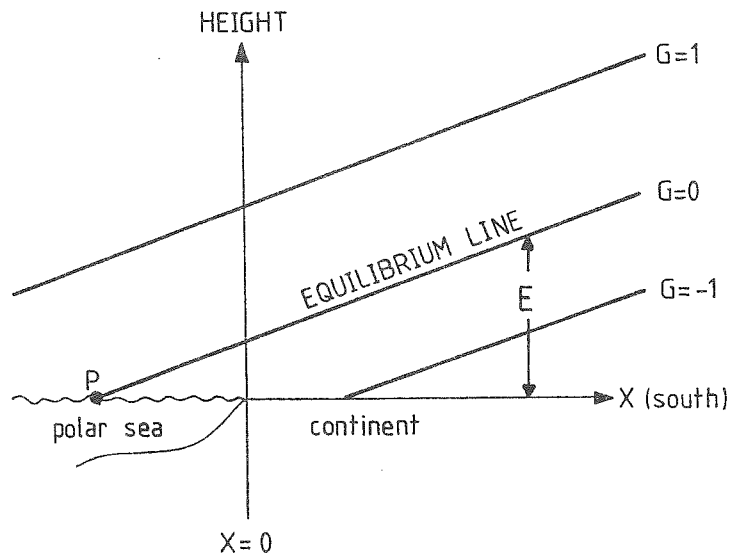


Fig. 15. An example of the mass-balance field. Unit is meter of ice equivalent (density $\simeq 900 \text{ kg/m}^3$) per year. The intersection of the equilibrium line with sea level defines the 'climate point' P .

The fact that the height dependence of G is expressed in $h-E$, and not in h , reflects the assumption that conditions at large surface elevation in the midlatitudes resemble those at small elevation in the subpolar regions. To give an impression of the accumulation rates involved: the Antarctic Ice Sheet receives about 0.3 m/yr (water equivalent), while precipitation (mostly snow) over the Arctic Basin is about 0.5 m/yr.

Fig. 16 shows two possible shapes of the height dependence of G . The thin line was used by Andrews and Mahaffy (1976) in studying the possibility of rapid growth of the Laurentide Ice Sheet. The solid line represents the height dependence adopted in this chapter. The parameters used are: $a=0.732 \cdot 10^{-3} \text{ yr}^{-1}$, $b=0.268 \cdot 10^{-6} (\text{m yr})^{-1}$, $h_c = E+1500 \text{ m}$ and $G_c = 0.5 \text{ m yr}^{-1}$.

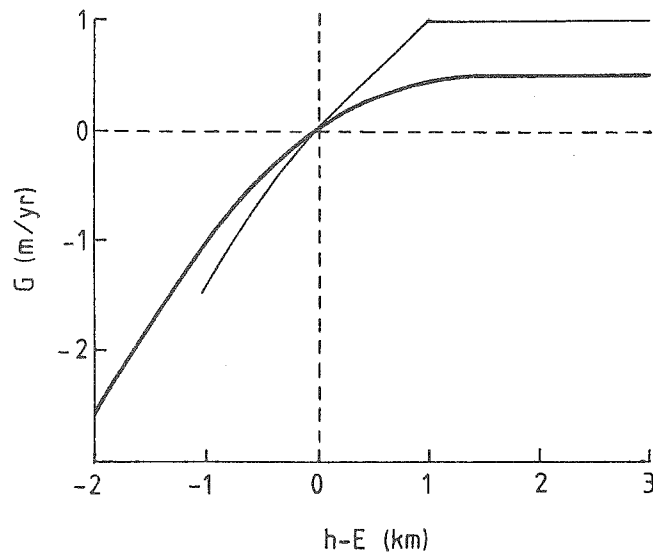


Fig. 16. Dependence of the mass balance on surface elevation. Heavy line: used in this analysis; thin line: used by Andrews and Mahaffy (1976) in a simulation of rapid growth of the Laurentide Ice Sheet.

The latitudinal dependence of G also suffers from uncertainty. Weertman (1961, 1976), for example, uses a value of 10^{-3} for χ . Sugden and John (1976; p. 88) suggest $\chi=0.78 \cdot 10^{-3}$. Data mapped by Charlesworth (1957) indicate a value of about $0.6 \cdot 10^{-3}$ for the northern half of Europe. Experiments with an energy-balance model for snow/ice melt (ref. [4], discussed later) give $\chi=0.35$ to $0.6 \cdot 10^{-3}$. This uncertainty in the value of χ is serious because the equilibrium size of the Northern Hemisphere ice sheets is very sensitive to it. There is one argument that makes a comparatively small value of χ preferable: during glacial conditions the latitude dependence of the surface albedo in the 40 to 70 °N latitude belt will be smaller. Consequently, the meridional gradient in surface temperature will also be smaller and this will certainly be reflected in a smaller value of χ .

To understand how the height-mass balance feedback affects the equilibrium state(s) of a Northern Hemisphere ice sheet, we will first discuss an analytical formulation of the problem. This has the advantage that the constants appearing in the expression for G need not be specified a priori (in numerical experiments discussed later, this is inevitable).

4.2 Solution diagram for a plastic ice sheet

To compute the evolution of an ice sheet it is necessary to know its mass balance. Given a mass-balance field $G(x,h)$, the elevation of the ice surface $H(x)$ is needed to obtain the the total mass balance of the sheet. A stability analysis will be much easier if a unique relation can be found between the total mass balance and the size (or volume) of the ice sheet. As will become clear below, such a relation exists if the ice flows as a perfectly plastic substance.

Plastic flow is characterized by the fact that two flow regimes occur: if the shear stress is smaller than some critical value no deformation takes place (zero strain rate), if the shear stress is larger than this critical value, deformation is extremely large. The critical value of the shear stress is called the yield stress. If the flow is active, i.e. stresses are continuously being built up, the property of plasticity tends to make stresses equal to the yield stress everywhere. This can be used to derive the profile of a perfectly plastic ice sheet. Assuming a flat base, the total horizontal force working on the ice-sheet base is proportional to $H(dH/dx)$. If the ice sheet is frozen to its bed, the shear stress at the base must also be proportional to $H(dH/dx)$. Thus in the case of plastic flow $H(dH/dx)$ is constant, from which it follows immediately that $H \propto \sqrt{x}$. Measurements on the Antarctic Ice Sheet have shown that such a parabolic profile fits observed profiles reasonably well. See Paterson (1969) for an extensive discussion on this point.

In the coordinate system used here the ice-sheet profile is given by (this equation was already used in section 3.3)

$$H(x) = \sigma \left[\frac{1}{2} L - \left| x - \frac{1}{2} L \right| \right]^{1/2}. \quad (17)$$

A yield stress of 1 bar gives a value of σ that is in agreement with the height-to-width ratio of the present large ice sheets.

The equilibrium size of a Northern Hemisphere ice sheet, bounded in the north by the polar sea, is again found by setting the average mass balance of its southern half (denoted by G^*) to zero (compare section 2.4). G^* is found by integrating $G(h,x)$ along the path $H(x)$,

that is

$$G^* = \frac{2}{L} \int_{L/2}^L G(x, H(x)) dx . \quad (18)$$

Equilibrium solutions follow from the requirement $G^* = 0$; they are stable if $\partial G^*/\partial L < 0$ and unstable if $\partial G^*/\partial L > 0$.

At this point $G(x, h)$ has to be specified. To keep things simple we assume that G depends linearly on height. For the following analysis this is justified, because the qualitative behaviour of the ice sheet is the same for a linear and parabolic dependence of G on height (see ref. [5] in which a parabolic dependence is also considered). So we write

$$G = (P-x)\beta\chi + \beta h , \quad (19)$$

where β is of order 10^{-3} yr^{-1} . Substitution of eqs. (17) and (19) in eq. (18) and carrying out the integration yields

$$G^*(L) = F_1 + F_2 L^{\frac{1}{2}} + F_3 L , \quad \text{with} \quad (20)$$

$$F_1 = \beta \chi P ,$$

$$F_2 = 0.47 \beta \sigma ,$$

$$F_3 = -0.75 \beta \chi .$$

Eq. (20) immediately shows that if β and χ are positive, i.e. if the mass balance increases with height and latitude, $\lim G^*(L \rightarrow \infty) = -\infty$. This means that the equilibrium ice-sheet size is finite (this is physically quite clear, of course).

Fig. (17) shows an example of a $G^*(L)$ curve. P has been set to zero, because varying P only shifts the curve up and down. Two equilibrium solutions exist: $L = 0$ and $L = 3500 \text{ km}$; the latter is stable. If P now decreases ($P < 0$, the climate point shifts into the polar sea), the $G^*(L)$ curve shifts downward and for some time the two equilibrium solutions still exist: a small unstable ice sheet and

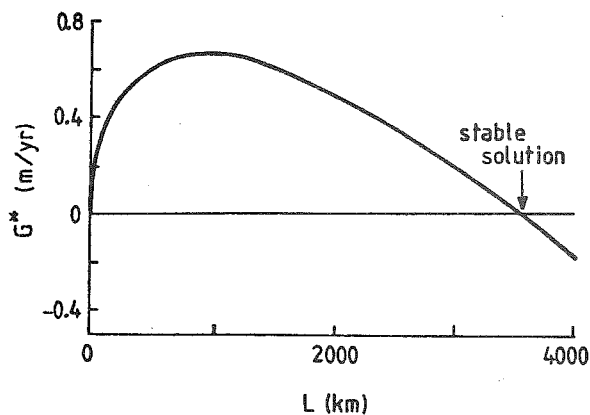


Fig. 17. Mean mass balance of the southern half of the plastic ice sheet (G^*) as a function of the ice-sheet size (L). Intersections with the line $G^*=0$ represent equilibrium states.

a larger stable ice sheet. If P is located far away from the continent, the $G^*(L)$ curve lies completely below the line $G^*=0$ and no ice sheets in equilibrium are possible. On the other hand, if $P > 0$ (the climate point is located on the continent) the $G^*(L)$ curve shifts upward and only one equilibrium state exists: a large stable ice sheet.

Adding to the foregoing considerations that $L=0$ is always a stable equilibrium solution if $P < 0$, we are now able to construct a solution diagram, i.e. to plot the equilibrium ice-sheet size as a function of P . The solutions of $G^*(L)=0$ are easily found by squaring eq. (20) and solving the resulting quadratic equation. This gives

$$L_{1,2} = \frac{F_1^2 - 2F_1F_3 \pm F_2 \sqrt{F_2^2 - 4F_1F_3}}{2F_3^2}, \quad (21)$$

from which $L_{1,2}$ can be computed for any parameter set P, σ, χ (note that the equilibrium solutions are independent of β).

Fig. 18 shows the solution diagram for $\sigma=2.5 \text{ m}^{\frac{1}{2}}$ and $\chi=10^{-3}$, $0.7 \cdot 10^{-3}$ respectively. The hysteresis due to the height-mass balance feedback comes out clearly; it is more pronounced if the slope of the equilibrium line is smaller. Apparently, we can distinguish between three regimes in the climatic conditions as follows:

- (i) warm conditions ($P < P_{\text{crit}}$) in which no equilibrium ice sheets are possible,

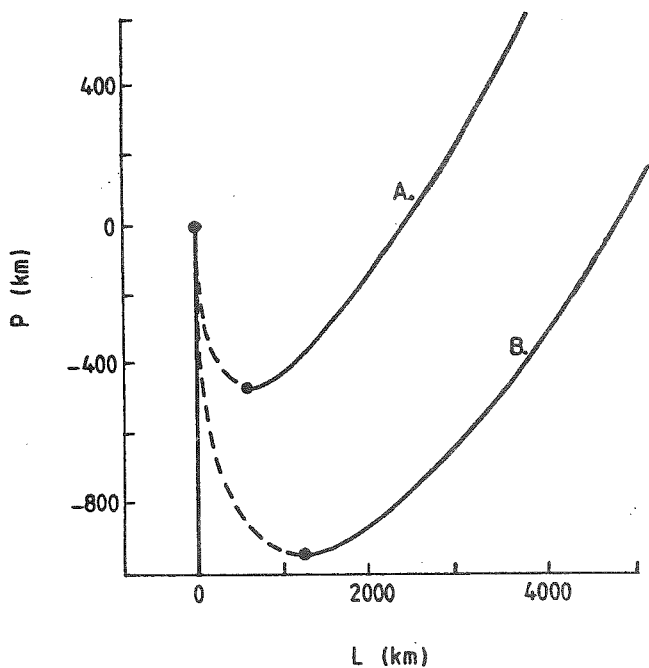


Fig. 18. Solution diagram for a Northern Hemisphere continental ice sheet flowing perfectly plastic. Solid lines represent stable equilibrium states, broken lines unstable ones. Critical points are indicated by dots; the lower one of a particular curve is referred to as P_{crit} in the text.

Curve A.: $\chi = 10^{-3}$
 Curve B.: $\chi = 0.7 \cdot 10^{-3}$

- (ii) moderate conditions ($P_{crit} < P < 0$) allowing two stable equilibrium states: $L = 0$, $L =$ a few thousand kilometers,
- (iii) cold conditions ($P > 0$), with a large ice sheet as the only possible stable equilibrium state.

The crucial point now is whether in reality P passes P_{crit} or not. To answer this question it is necessary to obtain a quantitative picture of how climatic variations affect the mass balance of an ice sheet. This will be discussed later in chapter 6.

Before comparing the solution diagram in Fig. 18 with that of a more sophisticated ice-sheet model (which has to be solved numerically), we examine the characteristics of the plastic model a little bit further. The critical point P_{crit} is found by equating the expression in the square root of eq. (21) to zero, yielding

$$P_{crit} = -0.074 (\sigma/\chi)^2 . \quad (22)$$

Apparently, the hysteresis is more pronounced when the height-to-width ratio of the sheet is larger or when the slope of the equilibrium line is smaller. Another impression of how changes in σ and χ affect the

ice-sheet size may be obtained by putting $P = 0$ in eq. (21). We then find for the size of the large stable ice sheet

$$L = 0.39 (\sigma/\chi)^2 . \quad (23)$$

So the ice-sheet size decreases with χ and increases with σ . In summary, we see that with regard to the solution diagram of the present ice-sheet model, the relevant parameter is σ/χ . This can be seen directly from eq. (20), of course.

4.3 Solution diagram for a flow model

In the case of perfect plasticity, the profile of an ice sheet is completely determined by its size. This implies that the profile only depends on the average mass balance over the sheet because this determines the ice-sheet size. Variations of G over the sheet do not influence the profile. In the following the constraint of perfect plasticity will be dropped by constructing an ice-sheet model in which the flow of ice is explicitly modelled, though in a rather crude way.

Horizontal ice-mass discharge is a consequence of two processes, namely, sliding of ice over the bedrock (basal sliding) and internal deformation within the ice. Nye (1959) proposed to use a general flow law for the vertically-integrated ice velocity which takes into account both basal sliding and internal deformation. It has the form

$$u = k \tau_b^m , \quad (24)$$

where u is vertical mean horizontal velocity, τ_b the shear stress at the base of the ice mass, and k and m are constants. The proposed value of m is 2 to 3, whereas k depends in principle on temperature. In fact eq. (24) is a form of Glen's law applicable to large ice sheets not undergoing extensive basal sliding.

Eq. (24) may be generalized to the two-dimensional case. Since the basal shear stress is proportional to $H \nabla H^*$, where H is ice thickness and H^* the elevation of the ice surface above sea level, the

vertically-integrated mass-flow vector becomes

$$\hat{M} = K H^{m+1} \left[\nabla H^* \cdot \nabla H^* \right]^{(m-1)/2} \nabla H^* \quad (25)$$

The evolution of the ice sheet is described by the conservation of ice mass, i.e.

$$\frac{\partial H}{\partial t} = \nabla \cdot \hat{M} + G \quad (26)$$

A more transparent way of formulating the model may be obtained by writing eq. (26) as a nonlinear diffusion equation:

$$\frac{\partial H}{\partial t} = \nabla \cdot D \nabla H^* + G \quad , \text{ with} \quad (27)$$

$$D = K H^{m+1} \left[\left(\frac{\partial H^*}{\partial x} \right)^2 + \left(\frac{\partial H^*}{\partial y} \right)^2 \right]^{(m-1)/2} \quad (28)$$

The diffusivity for ice mass D increases with the slope of the ice surface and in particular with the ice thickness, which is the reason that large ice sheets have steep edges. Eqs. (27) and (28), together with the condition that $H \gg 0$, form the basic model equations. They will be used in a study of the Scandinavian Ice Sheet (section 5.3).

In order to reduce computational times needed to integrate the model numerically, we introduce some simplifications. The x-axis is located along a meridian and is used for the explicit computation of the evolution of the ice sheet. However, we parameterize the ice-mass discharge in the y-direction as follows. If the x-axis is placed over the highest part of the ice sheet and if variations in bedrock height in the y-direction are small, we may apply the approximations $\partial H^*/\partial y = 0$ and $\partial^2 H^*/\partial y^2 = H/Y^2$. Inserting this in eqs. (27) and (28) leads to the following model equations:

$$\frac{\partial H}{\partial t} = \frac{\partial}{\partial x} \left[D' \frac{\partial H^*}{\partial x} \right] + D' H/Y^2 + G \quad , \text{ with} \quad (29)$$

$$D' = K H^{m+1} \left(\frac{\partial H^*}{\partial x} \right)^{m-1} \quad . \quad (30)$$

We thus end up with three constants that have to be prescribed: K , m and Y . In the experiments discussed here Y was set to 1000 km. The steepness of the ice-sheet edge is determined by m ; using $m=2.5$ appeared to give a steepness comparable to that of present-day ice sheets. The remaining constant K governs the height-to-width ratio of the sheet. To get an impression of how sensitive this ratio is to variations in K , we apply a scale analysis to the centre of the sheet. Inserting in eq. (29) $\partial H/\partial t = 0$, $Y = \infty$, $m = 2.5$, $H = H_0$ and $x = L_0$ (half-width of the sheet) yields

$$H_0 = (G/K)^{0.17} L_0^{0.58} \quad (31)$$

Given some ice-sheet size, H_0 is proportional to $K^{-0.17}$. A substantial change in K is thus needed to change the height of the ice sheet. Eq. (31) also shows that if the ice-sheet size is forced to be constant (e.g. the Greenland Ice Sheet which is bounded by ocean), its height is rather insensitive to the mass balance G (note that in the case of plasticity, H would be completely independent of G).

With the model described by eqs. (29) and (30) many numerical experiments were carried out. A detailed documentation of the basic behaviour of the model ice sheet can be found in ref.[6]. In this chapter we only discuss the solution diagram for a Northern Hemisphere ice sheet subject to the height dependence of G shown in Fig. 16. The constant K was chosen such that for $L = 2000$ km it gives about the same ice-sheet height as $\sigma = 2.5 \text{ m}^{\frac{1}{2}}$ gives in the plasticity case. The model was solved on a grid with a spacing of 70 km. Stable equilibrium solutions were obtained by integrating with a time step of 20 yr until a steady state was reached. The time needed to reach such a state varied from 20 to 70 ka (1 ka = 1000 years). For more detail on the numerical method of solution, see ref.[7].

Fig. 19 shows the solution diagram for this ice-flow model. The slope of the equilibrium line was set at $0.7 \cdot 10^{-3}$, so the solution curve can directly be compared to curve B. in Fig. 18. It is obvious that the behaviour of the flow model is qualitatively the same as that of the plasticity model. One difference should be noted, however. In the flow model, the sensitivity of L to climatic variations is

smaller. This results in a much smaller equilibrium ice-sheet size for cold conditions: for $P = 200$ km, the flow model gives $L = 2900$ km while the plasticity model yields $L = 5000$ km.

A few sample calculations brought to light that differences in the behaviour of the models are due to both the different formulation of the mass balance and the different treatment of the ice dynamics. Nevertheless, the comparison made above shows that the perfectly plastic ice sheet model does a good job: it reveals in a clear way how the height-mass balance feedback may create multiple equilibrium solutions in the cryosphere.

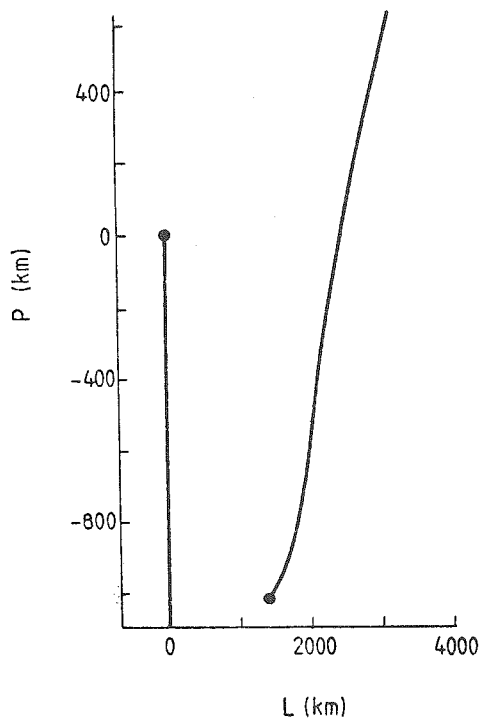


Fig. 19. Solution diagram for the flow model. Solid lines represent stable equilibrium solutions. Critical points are indicated by dots.

5. THE EVOLUTION OF THE NORTHERN HEMISPHERE ICE SHEETS

5.1 Were the ice sheets close to equilibrium ?

So far, the discussion has been restricted to steady states of a Northern Hemisphere ice sheet, but we cannot be sure that during a glacial maximum the Northern Hemisphere ice sheets were close to an equilibrium state (that is, in equilibrium with the climatic conditions that prevail during a glacial maximum). The oxygen isotope record (Fig. 1) gives some indication that this was not the case. The Carribean core, which has the largest resolution in time, in particular shows that just before the point where the global ice volume jumps back to a small value, the growth rate of the ice volume hardly slows down. Moreover, the fact that a critical ice volume seems to exist at which some instability mechanism destroys the ice sheets rapidly makes it unlikely that they reached an equilibrium state. In view of this, one has to be careful in using diagrams of equilibrium solutions like Fig. 19 in the construction of an ice age theory.

Concerning time scales of ice sheets, some confusion exists in the literature. Some authors mean a response time to a perturbed ice-sheet size, others have in mind a time scale for growth to equilibrium after a climatic cooling. In order to get some insight in how rapidly the Northern Hemisphere ice sheets may grow, we discuss in this chapter a few model experiments on ice sheet evolution.

Another aspect of the question posed at the head of this section is that of stochastic forcing of ice sheets. Since in the atmosphere flow instabilities are continuously present, the associated weather variability may act as a stochastic energy source for ice sheets. In principle, part of the variations in global ice volume or in the sizes of the Northern Hemisphere ice sheets may be due to random forcing by the atmosphere. Section 5.4 will be devoted to a brief discussion on this point.

5.2 Evolution of a one-dimensional model ice sheet

The ice-sheet model constructed in section 4.3 can be used to study the growth of a Northern Hemisphere ice sheet subject to various climatic conditions. In the following, the forcing of the ice sheet is formulated by specifying P as a function of time, but the structure of the mass-balance field discussed in section 4.1 is retained.

As a first experiment we consider the academic case of a sudden substantial climatic cooling at $t = 0$. This cooling is represented by setting $P = 350$ km during the whole integration. Fig. 20 shows the resulting ice sheet evolution for two values of the slope of the equilibrium line χ . Apparently, the equilibrium ice sheet size and the time scale for growth are larger if χ is smaller. For small χ , the average mass balance is positive but small for quite a long time. In this case the growth time of the sheet, being about 50 ka, is determined by the nature of the height-mass balance feedback and not by the ice flow mechanics.

A somewhat more realistic experiment is to apply a varying forcing to the model. For example, the precession of the equinoxes (period about 22 ka) has a large effect on summer insolation at high latitudes. To mimic this effect in a crude way, the model was forced by prescribing P as

$$P = -140 + 490 \sin(\pi t/10) \text{ km}, \quad (32)$$

where t is time in ka. According to eq. (32), the climate point moves back and forth over a distance of about 1000 km. Once in every 20 ka,

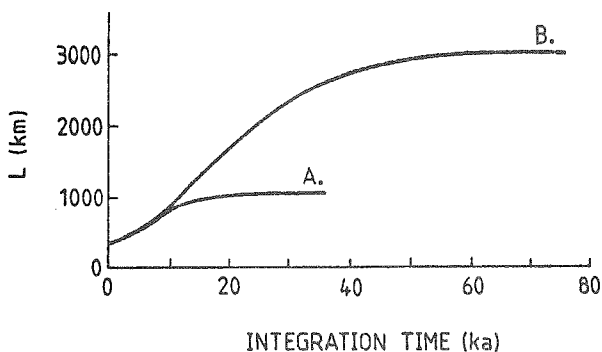


Fig. 20. Growth of a Northern Hemisphere model ice sheet after a sudden climatic cooling.

Curve A.: $\chi = 2 \cdot 10^{-3}$.

Curve B.: $\chi = 0.7 \cdot 10^{-3}$.

$K = 1 \text{ m}^{-3/2} \text{ yr}^{-1}$.

$Y = 1000 \text{ km}$.

the climate point is located on the continent for some time. This situation roughly reflects the conditions during a period of a large eccentricity of the earth's orbit around the sun. The amplitude of the movement of P corresponds to the same sensitivity of G to insolation variations as used by Weertman (1976).

The reaction of the model ice sheet to this periodic forcing is shown in Fig. 21. It is displayed in terms of the area of the meridional cross section through the sheet, defined by

$$AR = \hat{H} L = \int_0^L H(x) dx \quad . \quad (33)$$

\hat{H} is the average thickness of the ice sheet.

At first the ice sheet grows very slowly, but after about 20 ka the height-mass balance feedback becomes stronger and the ice-sheet volume increases more rapidly. After 60 ka a stable oscillation settles down around an ice sheet size of about 2500 km. So, although the average position of P is located in the polar sea, a large ice sheet forms and does not disappear again. The latter is an unfortunate result if one wants to explain the glacial cycles, but not surprising in the light of Fig. 19. We return to this point later.

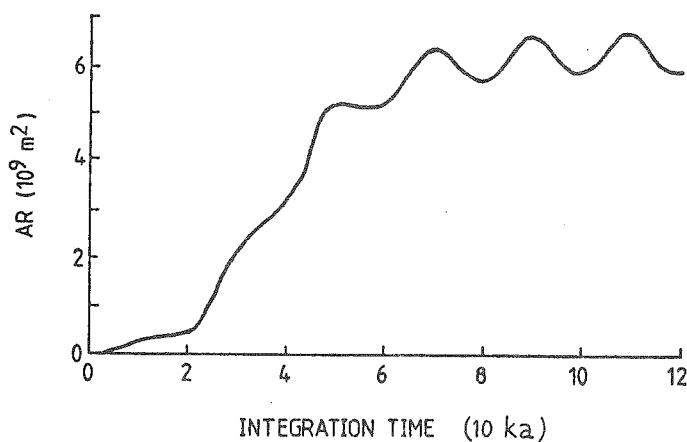


Fig. 21. Growth of a Northern Hemisphere model ice sheet subject to a periodic forcing. In this experiment $\chi = 0.65 \cdot 10^{-3}$, $K = 3 \text{ m}^{-3/2} \text{ yr}^{-1}$ and $Y = 1000 \text{ km}$.

5.3 Simulation of the growth of the Scandinavian Ice Sheet

The one-dimensional model employed in the last section uses a very schematic representation of the geometry of the Northern Hemisphere. In view of the large amount of computer time needed to run a two-dimensional model, the use of a one-dimensional model is inevitable in most experiments. Nevertheless, a few runs on ice-sheet growth were carried out with a two-dimensional model of the Scandinavian Ice Sheet. A detailed description of those experiments can be found in ref. [7].

The model is based on eqs. (27) and (28) and uses the height dependence of G described in section 4.1. However, the equilibrium line now becomes an equilibrium plane with a constant slope. This slope has a north-south and a west-east component, according to

$$E = 70(\varphi - 70) + 25\lambda - 300 \text{ m.} \quad (34)$$

In eq. (34), φ and λ are latitude and longitude expressed in $^{\circ}\text{N}$ and $^{\circ}\text{E}$ respectively. The west-east gradient in the mass-balance field is included to account for the higher accumulation rates observed near open sea (e.g. Chorlton and Lister, 1971). With respect to present-day conditions, eq. (34) represents a lowering of the equilibrium

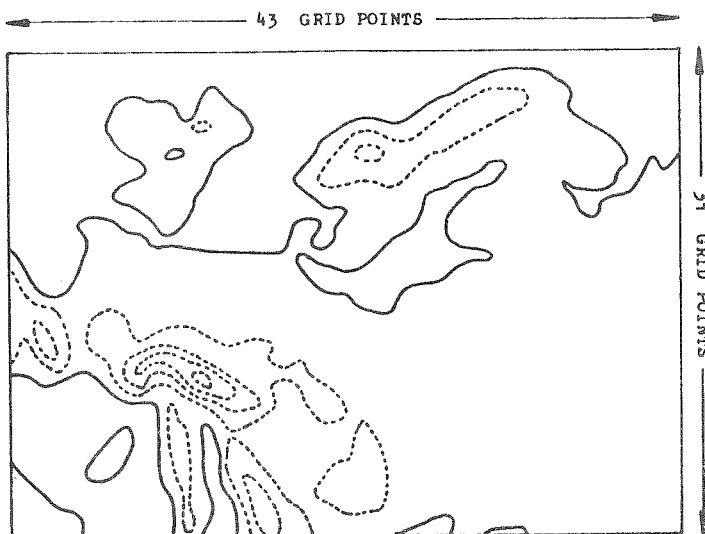


Fig. 22. Domain of the two-dimensional ice-sheet model. Europe is covered by 1333 grid points spaced at 100 km. The orography is indicated by broken lines spaced at intervals of 500 m.

plane by about 1000 m. It is hard to believe that in the quarternary epoch a larger sudden cooling ever occurred.

Fig. 22 shows the model domain, the grid size is 100 km. The distortion of distances by the map projection is corrected by means of a map factor in the difference scheme. The fixed bedrock elevation ξ is specified with respect to present-day sea level. Boundary conditions applied are: $H=0$ if $\xi < -200$ m (edge of the continental shelf), or if the grid point lies on the boundary of the model domain.

To obtain a lower limit of how rapid glaciation in Europe can take place, a run was carried out with the sudden climatic cooling described by eq. (34). Initial conditions were $H(t=0)=0$. Fig. 23 displays the resulting ice-sheet evolution. The Alps and the mountains of Scotland are soon covered with stable ice caps, but the Scandinavian Ice Sheet needs time to grow. After 5 ka the maximum ice thickness is found over the Scandinavian mountains, later over the Gulf of Bothnia. After about 30 ka the Scottish and Scandinavian sheets merge and the ice extent is close to the maximum extent observed in Europe during

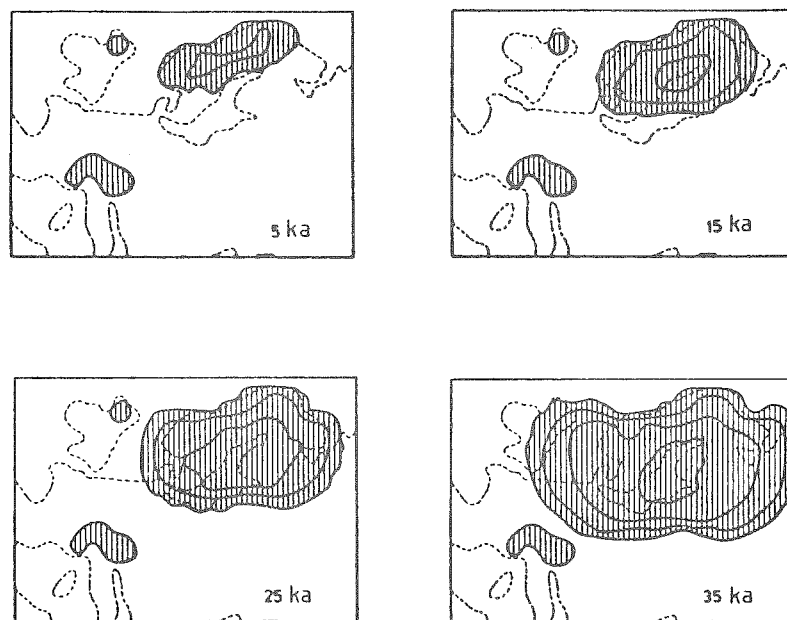


Fig. 23. Growth of the European ice sheets after a substantial cooling. Integration time is indicated in the panels. Contours of ice thickness (not of surface elevation) are represented by heavy lines; the contour interval is 1000 m.

during the Pleistocene (namely in the Riss glacial).

An impression of how the ice volume increases is given in Fig. 24. During the first 13 ka of the integration the growth rate is fairly constant, but then the ice volume starts to grow more rapidly. After 40 ka, the ice sheet still seems to be far from an equilibrium state, which reflects the extreme cold climatic conditions imposed. But even in such conditions a time span of at least 25 ka is needed to create an ice sheet of ice-age size. This makes the concept of rapid glacierization as proposed by several authors rather doubtful, unless an extremely strong positive feedback between ice-sheet size and accumulation of snow is assumed.

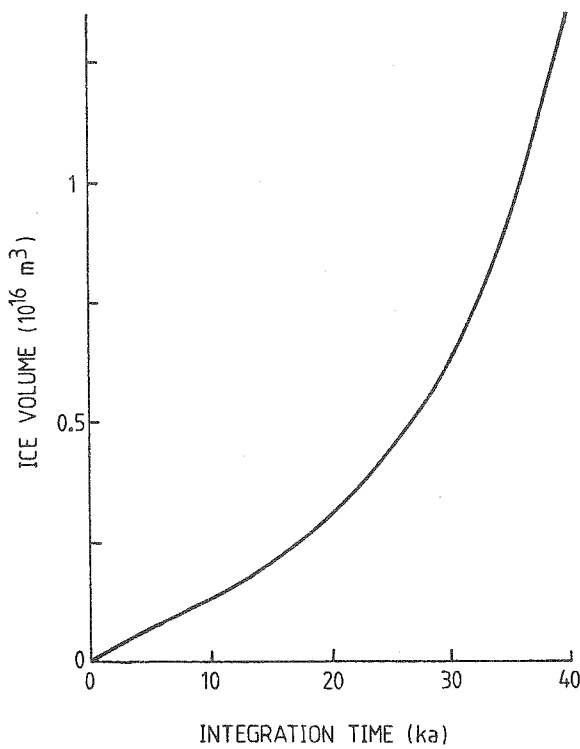


Fig. 24. Total ice volume in Europe as a function of integration time for the 'sudden cooling experiment'.

5.4 Stochastic forcing of ice sheets

From the viewpoint of a large ice sheet, short-term variations in the mass balance reflecting weather variability appear in a sequence of irregular pushes, or, in mathematical terms, constitute a stochastic forcing. Similar to Brownian motion, a large number of small pushes may lead to an unpredictable substantial growth (or decay) of the ice sheet. If there is no damping, i.e. a force that tries to drive the ice sheet back to its equilibrium size, the ice sheet may expand indefinitely or shrink to nothing. It is obvious that the reaction of ice sheets to stochastic forcing deserves to be investigated. An estimate of ice-sheet variability due to random forcing by weather fluctuations is needed in judging the performance of deterministic climate models.

A formal framework for stochastic climate models has recently been presented by Hasselmann (1976). Interesting applications have been published by Frankignoul and Hasselmann (1977) and Lemke (1977). A basic idea behind those stochastic climate models is that of time-scale separability. There is a large time scale in which one is really interested (the output of the system) and a small time scale on which the forcing acts (the input of the system). In the case of an ice sheet, this time-scale separation is rather clear: the evolution of the ice sheet takes place on the large time scale, while the daily or even yearly variations in the mass balance act on the small time scale.

Let us consider a Northern Hemisphere ice sheet in equilibrium with the climatic conditions represented by the mass-balance field described in section 4.1. Let us next imagine that the climate point P moves north- and southward at random. We may then ask the question: How will the ice-sheet size L react to this stochastic forcing? Will there be a substantial variability in L for a realistic strength of the forcing? In the following, we will try to find an answer by using a simple linear model for the interaction between ice-sheet size and climate point variability.

As a start, we assume that the time-dependent behaviour of an ice sheet may be written

$$\frac{dL}{dt} = f(L,P) \quad (35)$$

Note that the function f is not completely equal to the mass balance because the left-hand side of eq. (35) represents the time derivative of the ice-sheet size instead of that of the ice-sheet volume. Linearization around some equilibrium state L_0 (corresponding to climatic conditions P_0) yields

$$T_r \frac{dL'}{dt} = -L' + P' \left. \frac{\partial L}{\partial P} \right|_{L_0, P_0} \quad (36)$$

Primes denote deviations from the equilibrium state. The relaxation time T_r is given by $-(\partial f / \partial L)^{-1}$ in $L=L_0$. If $P'(t)$ now represents a stationary time series, $L'(t)$ will also be stationary. Moreover, the linearity of the equation assures that if $\overline{P'(t)} = 0$, then $\overline{L'(t)} = 0$. Here, the overbar denotes an average over a sufficiently long time interval.

The variance of the ice-sheet size can be found by a Fourier transform of eq. (36) and subsequent integration of the resulting spectrum over all frequencies. If the random movement of the climate point is represented by a white-noise process $P'(t)$, the variance of the ice-sheet size becomes

$$\overline{L'^2} = \pi T_r \left[\frac{1}{T_r} \frac{\partial L}{\partial P} \right]^2 S_P \quad (37)$$

where S_P is the constant spectral level of the white noise. To compute an estimate of $\overline{L'^2}$, we can derive values for T_r and $\partial L / \partial P$ from an ice-sheet model. However, we also need an estimate of S_P .

In a first approximation, the climate point P follows some surface isotherm. Looking along a meridian, this isotherm will move north and southward. The mean distance over which it moves may be used as an estimate of the strength of the white-noise forcing. To be able to derive such an estimate from observational data (namely, interannual variability) we define a new random process by

$$P^*(t) = \frac{1}{T} \int_{t-\frac{1}{2}T}^{t+\frac{1}{2}T} P'(t') dt' \quad (38)$$

Here, T is the time interval over which the observations are averaged. The constant spectral level S_p of $P^*(t)$ is related to the variance of $P^*(t)$ according to

$$S_p = T \overline{P^*(t)^2} / \pi . \quad (39)$$

Finally, inserting this in eq. (37) yields

$$\overline{L'^2} = \frac{T}{T_r} \left[\frac{\partial L}{\partial P} \right]^2 \overline{P^{*2}} . \quad (40)$$

Employing data on inter-annual variability (so $T=1$ yr) given by Oort (1977) yields $\overline{P^{*2}} = 60\,000 \text{ km}^2$. This corresponds to a typical meridional shift of isotherms of about 250 km. Table IV shows the resulting estimate of σ_L , the standard deviation of the ice-sheet size. Estimates are given for the plastic model (section 4.2) and for the flow model (section 4.3); in both cases $P_o = -600 \text{ km}$ and $\chi = 0.0007$. Values of $\partial L/\partial P$ can be obtained directly from Figs. 18 and 19; values of T_r were derived by working out eq. (35) for the plastic model, and by a numerical experiment for the flow model.

	L_o	$\left[\frac{\partial L}{\partial P} \right]^2$	T_r	σ_L
plastic model	3200 km	12.25	10 ka	8.5 km
flow model	2000 km	0.36	15 ka	0.4 km

Table IV. An estimate of the standard deviation of the ice-sheet size due to stochastic forcing by weather fluctuations, according to the perfectly plastic model and the numerical flow model

The variability of the ice-sheet size obtained in this way is small, in particular for the flow model. The situation will change if feedback occurs between the ice-sheet size and the climatic conditions. If positive feedback exists, i.e. if the climate point moves southward if the ice-sheet size increases and vice versa, σ_L will be larger. A model incorporating this type of feedback is described in ref.[8]. Results of this model indicate that in the case of strong feedback the ice-sheet size will have a standard deviation of the order of a few hundred kilometers.

6. AN ESTIMATE OF ICE/SNOW MELT VARIATIONS

6.1 Introduction

So far climatic variations have been represented by changes in the position of the climate point P. We have investigated how the Northern Hemisphere ice sheets react to such changes. To relate the behaviour of ice sheets to insolation variations, it is necessary to look in some detail to how the mass balance reacts to changes in incoming solar radiation. This is probably the most difficult problem in physical modelling of the ice ages. In particular rain and snowfall are difficult to deal with because precipitation is linked closely to the atmospheric circulation. At present, this point can only be studied with general circulation models of the atmosphere, but even then a large uncertainty about predicted precipitation distributions exist. A clear illustration of this can be found in Heath (1979), who compared simulations of the ice-age climate by three different general circulation models. Although all models give a substantially lower amount of global precipitation, the distributions show large differences. Given this fact, no attempt was made to model precipitation in terms of ice-sheet size or the like.

A process that can be treated somewhat easier is melting of ice and snow. It is possible to study ice/snow melt with a comparatively simple model of the energy balance of the surface layer. Insolation variations can then be imposed to see how ice/snow melt changes.

In this chapter we will develop an ice/snow melt model. The results of several runs with this model will be employed to derive a parameterization of mass-balance variations in terms of absorbed solar radiation.

6.2 A simple model for the computation of ice/snow melt

Consider a surface layer consisting of ice and snow of some thickness, with heat capacity C. In the absence of heat transfer from or to deeper layers, the energy balance of the surface layer reads

$$C \frac{dT}{dt} = (1-a) Q - \tau \sigma T^4 - EF \quad . \quad (41)$$

In eq. (41), T is the temperature of the surface layer, t local time, a the effective albedo and Q the insolation at the top of the atmosphere. The constant τ represents an effective transmissivity of the total atmosphere for long wave radiation originating at the surface and thus includes the effect of counter radiation and surface emissivity; σ is the Stefan-Boltzmann constant. EF denotes the energy flux to the atmosphere by turbulent processes; it is parameterized by

$$\begin{aligned} EF &= e(T - T_a) && \text{if } T \geq T_a \\ EF &= 0 && \text{if } T < T_a \end{aligned} \quad (42)$$

Here, e is an exchange coefficient and T_a denotes air temperature at some height above the surface. No distinction is made between the latent and sensible heat flux, it is assumed that the total energy flux can adequately be described by the bulk formula (42). The air temperature depends on surface elevation according to

$$T_a(h) = T_a(0) - h\Gamma, \quad (43)$$

where Γ is the atmospheric lapse rate (6 K/km in this analysis). A major difficulty in this parameterization is that $T_a(0)$ has to be prescribed because it is not carried as a dependent variable (this would require the inclusion of a boundary-layer model, which would create new modelling problems; apart from this, such a model would be too time consuming to carry out integrations over 200 ka or so). Throughout the experiments with this model, $T_a(0)$ is set to the melting point. This may appear as an extremely crude approximation, but here one should realize that we are interested in melting, i.e. in conditions with high insolation only. The fact that in summer surface air temperature over the Arctic basin is close to the melting point lends some support to the use of $T_a(0) = 0^\circ\text{C}$.

In the present model, no refreezing of melt water takes place. As soon as T reaches the melting point, all surplus energy is used for melting of snow and ice and the melt water runs off immediately. An alternative approach hardly exists because the structure of the surface layer is unknown.

The effective albedo is computed from

$$(1-a) = (1-\alpha)(1-0.6 n^3)(0.6+0.2 \sin \psi), \quad (44)$$

where α is the surface albedo, n fractional cloud cover, ψ the solar zenith angle. The clear-sky transmissivity for short wave radiation (last term in parenthesis) was taken from Lumb (1964), the cloudiness factor from Laevastu (1960). The surface albedo runs from 0.9 for $\psi=90^\circ$ (low sun) to 0.6 for $\psi=0^\circ$ (high sun).

The model is numerically solved by a simple forward time scheme, with a time step of 15 minutes. It is forced by a stationary daily cycle in insolation (representative for a particular month and latitude) and integrated until a stable daily cycle in T is reached. With suitable initial conditions, this takes a few days of simulation. To obtain the yearly amount of ice/snow melt, a stable daily cycle is computed for each month.

6.3 Results for present-day insolation

Fig. 25 shows some typical daily cycles in T computed with present insolation. Solid curves apply to a surface elevation of 1500 m, dashed curves to sea level. Parameter values used are given in the figure caption. The values of e and C have been chosen such that reasonable melting rates result. As expected, the amplitude of the daily cycle increases with elevation and decreases with latitude.

Fig. 26 shows the yearly melting M as a function of latitude and height. The picture looks very reasonable, which is of course due to the choice of e and C . The overall magnitude of M is determined by the heat capacity of the surface layer. The latitudinal dependence of M stems from the decreasing insolation and the increasing mean effective albedo. The height dependence of M is due to the turbulent energy flux EF : at large elevations the atmosphere is so cold that the energy gained by the surface layer is immediately lost to the air above it, thus preventing T to reach the melting point.

Except for the order of magnitude, it is difficult to verify the computed distribution of M . It can hardly be expected that present-day conditions over Greenland and Antarctica are representative for

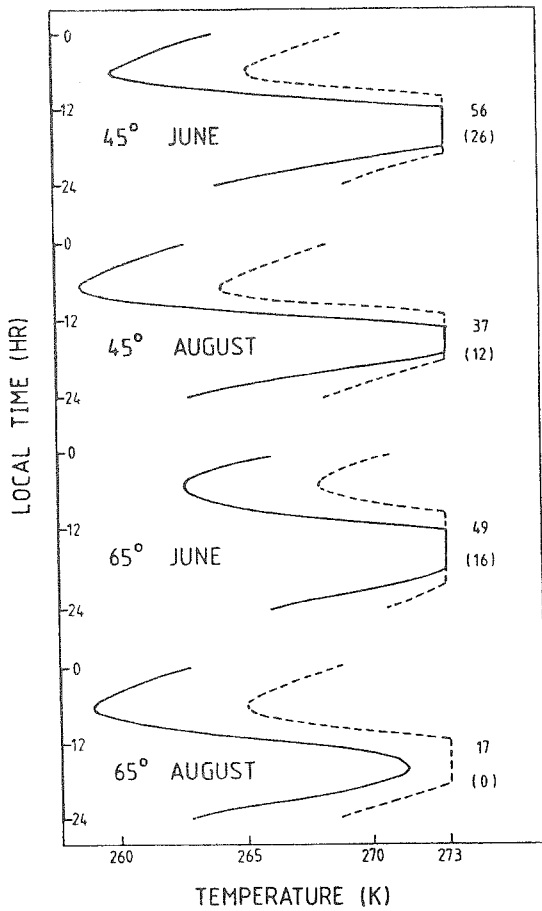


Fig. 25. Examples of daily cycles in T at a surface elevation of 1500 m (solid line) and at sea level (broken line). Numbers on the right-hand side of each curve give ice/snow melt in cm ice equivalent per month; numbers in parenthesis apply to 1500 m.

Parameter values used:

$$\begin{aligned}
 n &= 0.6 \\
 \tau &= 0.14 \\
 C &= 2 \cdot 10^5 \text{ J/(K m}^2\text{)} \\
 \Gamma &= 6 \text{ K/km} \\
 e &= 7 \text{ W/(K m}^2\text{)}
 \end{aligned}$$

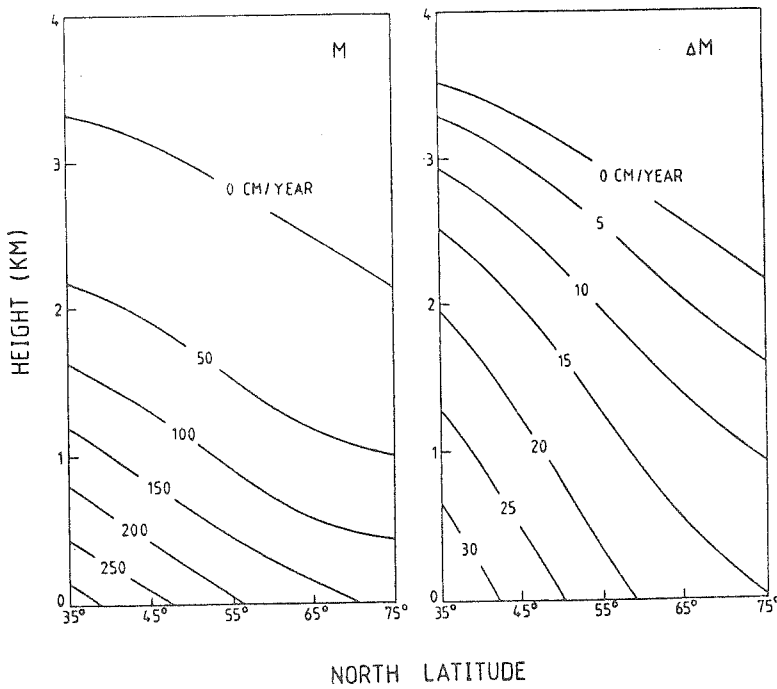


Fig. 26. Left panel: yearly ice/snow melt in cm ice equivalent per year, as a function of surface elevation and latitude.

Right panel: change in M for a 5% increase in insolation.

conditions that prevailed over the Laurentide and Eurasian ice sheets. This also applies to measurements over mountain glaciers. Consequently, no effort was made to fit the output of the melt model to specific observational studies. For the present purpose, namely to obtain an estimate of how ice/snow melt may vary due to insolation variations, we accept the distribution of M shown in Fig. 26 as a reasonable approximation to reality.

6.4 Model response to varying insolation

In a first sensitivity experiment, the solar constant was increased by 5%. This means that at each location the incoming radiation at the top of the atmosphere is 5% more. The resulting increase in the yearly ice/snow melt M is shown in the right panel of Fig. 26. We see that this increase is larger for larger M , which may be expected.

With regard to the astronomical ice-age theory, a more relevant experiment is to impose the Milankovitch insolation variations. To be able to do so, three orbital parameters of the earth are needed:

- (i) the eccentricity of the orbit around the sun,
- (ii) the longitude of the perihelion,
- (iii) the tilt of the earth's axis with respect to the ecliptic.

Those parameters change continuously which causes the insolation variations. Berger (1978) has provided very handy expansions of the orbital parameters in terms of Fourier series. In the present computations, ten terms in each expansion were retained which should give sufficient accuracy.

For the last 200 ka, yearly amounts of ice/snow melt were computed as a function of latitude and surface elevation. The model produces a considerable amount of interesting output, but here we will only look at a few results. Fig. 27 shows in a time-height diagram how melting rates varied during the last 200 ka according to the model. Results are shown for two latitudes: $\varphi = 65^\circ \text{N}$ and $\varphi = 50^\circ \text{N}$. The most striking feature in Fig. 27 is that, at least for the radiation variations of interest, the height dependence of M is quite well conserved with respect to some isoline (e.g. the 1 m/yr melt line). This is a convenient property if M has to be parameterized.

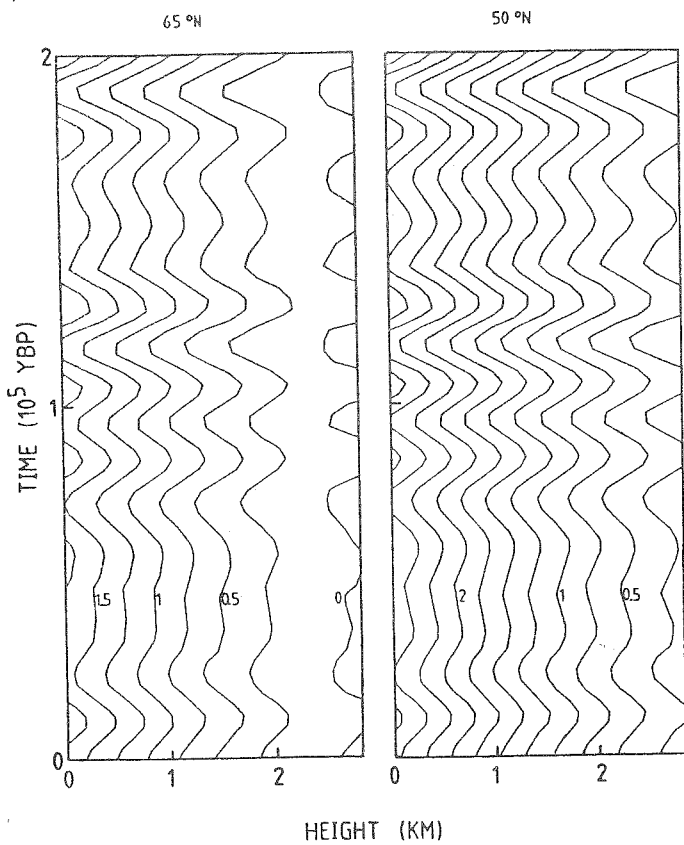


Fig. 27. Yearly ice/snow melt for the last 200 ka according to the model. Model parameters are slightly different from those used in Figs. 25 and 26. Unit is m of ice equivalent per year.

Table V. Values of $\partial M / \partial Q_a$, i.e. the sensitivity of yearly ice/snow melt to yearly mean solar radiation absorbed at the surface. Unit is m/yr per W/m^2 .

		Latitude			
		40°	50°	60°	70°
h = 0	m	0.139	0.133	0.116	0.106
h = 1500	m	0.138	0.114	0.088	0.058

Table V shows how sensitive M is to changes in yearly amount of absorbed solar radiation at the surface (denoted by Q_a). Values of $\partial M/\partial Q_a$ were obtained by computing linear regressions between M and Q_a over the last 200 ka. One should note that such regressions are not uniquely determined. In principle, a change in Q_a can be due to a change in insolation, yearly cycle, daily cycle, or a combination of these factors. For the present purpose, however, this plays no role: variations in Q_a are essentially due to variations in insolation. Of course insolation variations can have a different effect on M through the differences in daily and yearly cycle that are already present. Differences in sensitivity shown in Table V are in fact the result of this point. It appears that lower latitudes are more sensitive than higher latitudes, in particular at higher elevations.

The precession of the equinoxes and the obliquity variations have their strongest effect on the insolation at high latitudes. On the other hand, due to a smaller mean solar angle and consequently a larger mean effective albedo, a change in insolation affects Q_a at lower latitudes stronger than at high latitudes. Together with the fact that lower latitudes are somewhat more sensitive to changes in Q_a , this means that changes in ice/snow melt not necessarily increase with latitude, although insolation variations do. Moreover, the model showed larger variations in M at lower latitudes for the last 200 ka (this would not be different for other periods). The net result is that in a first approximation insolation variations shift the whole ice/snow melt field north- and southward, i.e. the latitudinal dependence of M is conserved (note that this requires a larger change in M at lower latitudes because $\partial M/\partial \varphi$ decreases with latitude). This finding justifies to some extent the approach used by Weertman (1976), who shifted the equilibrium line in his model north- and southward with insolation. More specifically, he coupled the point where the equilibrium line intersects sea level (called the climate point in this study) to a fixed amount of incoming solar radiation in summer. This leads to a maximum shift of the climate point over 14° latitude in the last 200 ka. The results of the ice/snow melt model indicate a value of about 10° latitude, however. For comparison: the amount of yearly mean absorbed radiation shifts over about 4° latitude.

6.5 Parameterization of mass-balance variations

In integrations with an ice-sheet model, to be discussed in chapter 7, the total mass balance has to be known. So both accumulation and melting due to rainfall should be taken into account. As noted earlier, this is an extremely difficult task. By lack of a sound alternative, the best thing to do seems to keep the precipitation effect constant. Variations in the mass balance are then completely due to changes in ice/snow melt caused by insolation variations. In this section a parameterization of the mass balance will be derived which is based on the results of the ice/snow-melt model.

As demonstrated in the foregoing section, the height dependence of M is quite well conserved with respect to the 1 m/yr melt isoline. It also appeared that this height dependence can adequately be represented by a parabolic curve. This leads to the expression

$$M(h) = c_1(h-h^*) + c_2(h-h^*)^2 + 1 \text{ m/yr} \quad (45)$$

$$\text{with } c_1 = -0.9 \cdot 10^{-3} \text{ yr}^{-1},$$

$$c_2 = 0.16 \cdot 10^{-6} \text{ (m yr)}^{-1}.$$

In eq. (45), h^* is the height at which M equals 1 m/yr. Variations in melting are now reflected by variations in h^* , according to

$$h^* = h_o^* + \gamma(Q_a/Q_{ao} - 1) \text{ m.} \quad (46)$$

Q_{ao} and h_o^* denote yearly mean absorbed solar radiation and height of the 1 m/yr melt line for present conditions. The sensitivity parameter γ depends on latitude:

$$\gamma(\varphi) = 44(80-\varphi) + 5000 \text{ m.} \quad (47)$$

Eqs. (45)-(47) completely describe the mass-balance variations due to insolation variations in terms of the amount of absorbed solar radiation at the particular latitude where a value of M is required. Q_a is easily obtained by evaluating the integral

$$\int_{\text{year}} Q(1-a) dt . \quad (48)$$

Note that the effective albedo a depends on the solar zenith angle.

To arrive at the total mass-balance field we proceed as follows. While ignoring the height dependence of the precipitation effect, we retain the latitudinal dependence by setting

$$h_o^* = \text{constant} + \mathcal{X} \varphi . \quad (49)$$

So \mathcal{X} represents the slope of the ice/snow melt isolines for present-day conditions. The total mass balance is written

$$G(h, \varphi) = M(h, \varphi) + Z , \quad (50)$$

where Z is a constant. The value of Z determines the critical insolation value at which a model ice sheet starts to develop. An upper limit is set to the mass balance by requiring that G is smaller than or equal to G_{lim} , where G_{lim} is of the order of 0.5 m/yr. This procedure is suggested by present-day precipitation rates over Antarctica and the Arctic basin (see section 4.1).

The parameterization of the mass balance described above will be employed in subsequent experiments with the Northern Hemisphere ice sheet model. The important parameters in this parameterization are \mathcal{X} (affecting the growth rate and the equilibrium size of the ice sheet), Z (affecting the glaciation threshold) and G_{lim} (affecting the growth rate). Of course these parameters do not act completely independently, the statements within parenthesis only indicate their major influence.

7. MODEL SIMULATION OF THE PLEISTOCENE GLACIAL CYCLES

7.1 Outline of the problem

In chapter 4 we found that for a wide range of climatic conditions a Northern Hemisphere ice sheet has two equilibrium states: $L = 0$ and $L =$ a few thousand kilometers. In terms of the position of the climate point P , the critical points of the hysteresis (black dots in Figs. 18 and 19) lie about 1000 km apart. For a sequence of glacials and interglacials to become possible, the climate point should thus move north- and southward over at least 1000 km. Due to the inertia of the ice sheet and the fact that insolation variations act on a time scale of 10 ka or so, we may expect that a much larger distance is required. Unfortunately, the results of the foregoing sections indicate that P shifts over about 10° latitude, which corresponds to a distance of only slightly more than 1000 km. This implies that the ice-sheet model described in section 4.3 is not capable of producing a sequence of glacials and interglacials when the Milankovitch insolation variations are imposed. This point was already demonstrated by the experiment with periodic forcing discussed in section 5.2. Many experiments were carried out to see whether changes in the model parameters (within realistic ranges) together with enhanced amplitude of the periodic forcing could change this situation. This was not the case: once the model produces a full-size ice sheet, it never disappears again. A climatic warming of a completely unrealistic strength appears to be necessary to initiate the decay of the ice sheet.

At this point we recall the discussion of the oxygen isotope record (section 1.2; Fig. 1). It was noted that the 100 ka cycle is asymmetric, i.e. deglaciation occurs within 10 ka while the built-up of new sheets requires 50 to 100 ka. Another point appearing in Fig. 1 is the fact that just before deglaciation starts, the growth rate of the ice volume hardly decreases. This suggests that during the glacial maxima the Northern Hemisphere ice sheets were not in equilibrium with the prevailing mass-balance conditions. It therefore seems likely that the deglaciations have to do with an inherent instability

of the cryosphere. A model designed to simulate the ice-volume record should thus include this instability.

Mechanisms that might explain such unstable behaviour are extensive ice-sheet surging and bedrock sinking due to the load of ice mass. Both processes were mentioned by Weertman (1961) as possible candidates for the explanation of the 'observed' speed with which deglaciations take place.

So far, studies on the surging of large ice sheets have been of a rather speculative nature. For example, periodic surging of the Antarctic Ice Sheet has been proposed as the cause of the Pleistocene glacial cycles (e.g. Hollin, 1972); we return to this point in chapter 8. Modelling of ice sheet and glacier surging is in rapid progress (e.g. Budd and McInnes, 1975) and one may hope that in the near future the role of ice-sheet surging in the climate system can be assessed.

Bedrock sinking is somewhat easier to deal with than ice-sheet surging. In the plastic ice-sheet model of Weertman (1976), isostatic adjustment of the bedrock takes place instantaneously, but this cannot create an instability of the type we are looking for. In Weertman (1961) the possibility of rapid ice-sheet decay caused by bedrock sinking is already mentioned, but, as he states, 'If this mechanism is to be effective, however, the time for isostatic sinking to occur must be longer than the time required to build up a large ice sheet'. In the following sections we will discuss some model experiments in which time-dependent bedrock adjustment is included. The results will show that this statement is not necessarily true.

Apart from the problem of understanding rapid deglaciations there is another unexplained aspect of the ice-volume record, namely, the dominance of the 100 ka cycle. The astronomical forcing on this time scale (variations in eccentricity) is small compared to that on the 40 and 20 ka time scales (variations in obliquity and precession of the equinoxes). Nevertheless, the power spectra of ice-volume records are dominated by a peak at about 100 ka (Hays et al., 1976). So far model experiments have failed to reproduce the power in the 100 ka time scale (Weertman, 1976; Pollard, 1978; Calder, 1974; Imbrie and Imbrie, 1980). In the following sections we will deal extensively with the problem of simulating the 100 ka cycle.

7.2 Incorporation of simple bedrock dynamics

To be able to include the effect of ice load on the bedrock elevation, we have to consider flexure of the lithosphere. Let us assume that an ice sheet rests on a lithospheric plate which behaves as a thin elastic shell. If the horizontal scale of the load is large compared to the thickness of the shell, the deflection ζ (positive downwards) of the lithosphere is governed by (e.g. Turcotte, 1979)

$$-D \nabla^4 \zeta - g \delta \rho \zeta = p . \quad (51)$$

Here, D is the flexural rigidity, $\delta \rho$ the difference in density between the displaced mantle rock and the replacing material (ice in the present case), g the acceleration of gravity and p the load per unit area. The first term in eq. (51) represents the upward force due to the rigidity of the lithosphere, the second term the hydrostatic force.

A suitable value for D is $0.5 \cdot 10^{24} \text{ kg m}^2/\text{s}^2$ (Turcotte, 1979). If the characteristic ice-sheet size is 10^6 m , the first term has an order of magnitude of $-0.5 \zeta \text{ kg}/(\text{m s})^2$. The ratio of the first to the second term thus equals $0.5/(g \delta \rho)$. Since $\delta \rho \simeq 2000 \text{ kg/m}^3$, it is obvious that the first term in eq. (51) can be neglected: the system is in hydrostatic equilibrium. For small ice sheets (smaller than 100 km, say) this approximation is not valid, but since we are mainly interested in large sheets it is reasonable to employ it.

Eq. (51) represents a steady state. For time integrations with the ice-sheet model, however, the time-dependent behaviour of the bedrock elevation is needed. In the most simple representation, the evolution to hydrostatic equilibrium may be written

$$\frac{d\zeta}{dt} = \frac{-1}{q\theta^*} (H+q\zeta) , \quad (52)$$

where H is ice thickness, $q = \rho_{\text{rock}}/\rho_{\text{ice}}$, and θ^* is the time scale for the isostatic adjustment. In the steady state, $\zeta = -H/q$.

Since the rock density of the upper mantle is about three times that of ice, $q=3$ is appropriate. This value was also used by Weertman (1976).

7.3 The effect of bedrock sinking

To get insight in how the sinking bedrock effects the ice-sheet evolution, a number of experiments were carried out with various values of the model parameters. In all runs the same periodic forcing as used in section 5.2 was imposed. Fig. 28 shows some typical results. The upper panel shows a model run in which no sinking of the bedrock was allowed ($\theta^* = \infty$). The second panel reveals the dramatic impact of bedrock sinking ($q=3$ in this experiment): after 90 ka the ice sheet disappears completely. With regard to the discussion in section 7.1, this seems to be a very promising result. Although the forcing is on a time scale of 20 ka, the dominant time scale of the model output is much larger and comparable to that of the glacial cycles appearing in Fig. 1. Furthermore, the model produces a glacial cycle that is asymmetric, which is also in agreement with the observational evidence. A substantial change in θ^* does not change this result in an essential way (third panel). If θ^* is still further reduced, a point is reached where the ice sheet cannot survive the insolation maxima (lower panel). In this case the bedrock sinking cancels the feedback between ice-sheet thickness and mass balance completely and a large ice sheet cannot be established.

The physical mechanism behind the behaviour of the ice sheet can be summarized as follows. As soon as the climate point reaches the continent, an ice sheet starts to grow. The growth rate depends on the feedback between ice thickness and the mass balance field, as discussed in detail in previous sections. Sinking of the bedrock lowers the ice-sheet surface and thus tries to cancel this feedback. Therefore the ice sheets grows rather slowly. If the ice sheet becomes thicker, the bedrock sinking will become more pronounced. A point may be reached where the average mass balance becomes negative, initiating the decay of the ice sheet. Due to the asymmetry in the

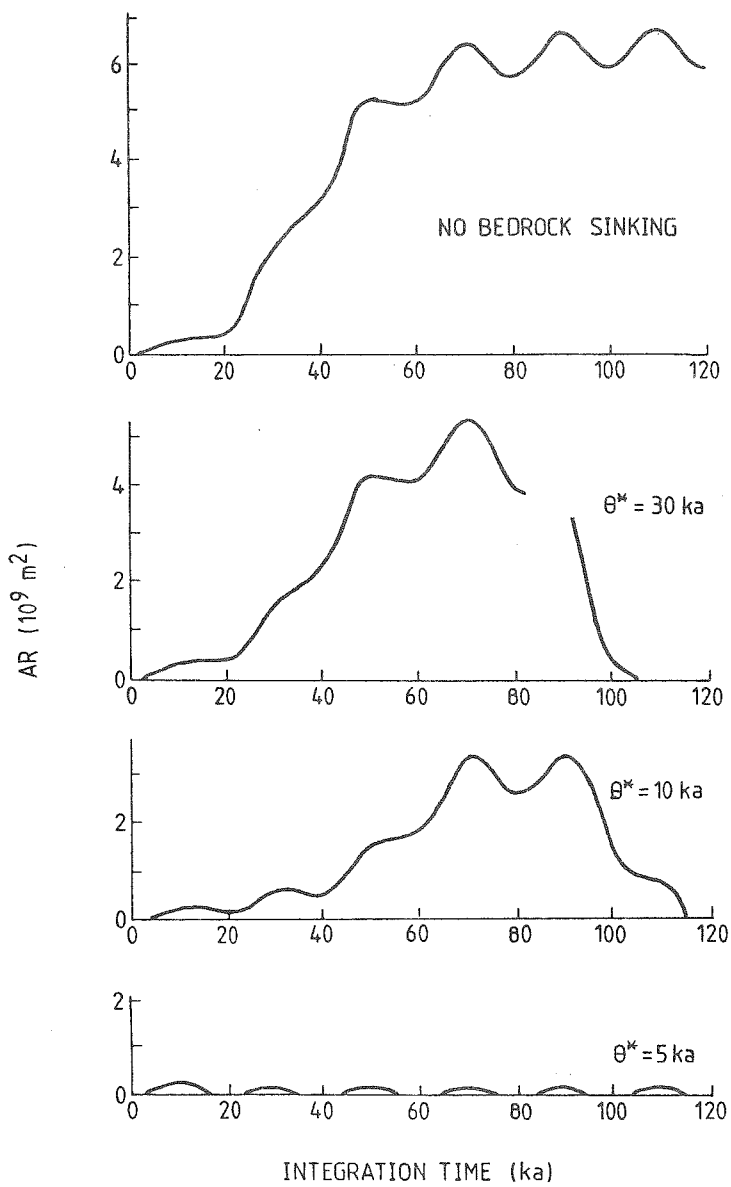


Fig. 28. Several model runs showing the effect of bedrock sinking in the case of periodic forcing with a period of 20 ka. AR is a measure of the ice-sheet volume, it is defined in eq. (33).

mass balance field (accumulation is strongly limited whereas ablation is not, see Fig. 16), the ice sheet may disappear completely within 10'ka. While the ice sheet melts, the bedrock will gradually start to rise again. However, this takes place too slowly to prevent complete melting of the ice sheet.

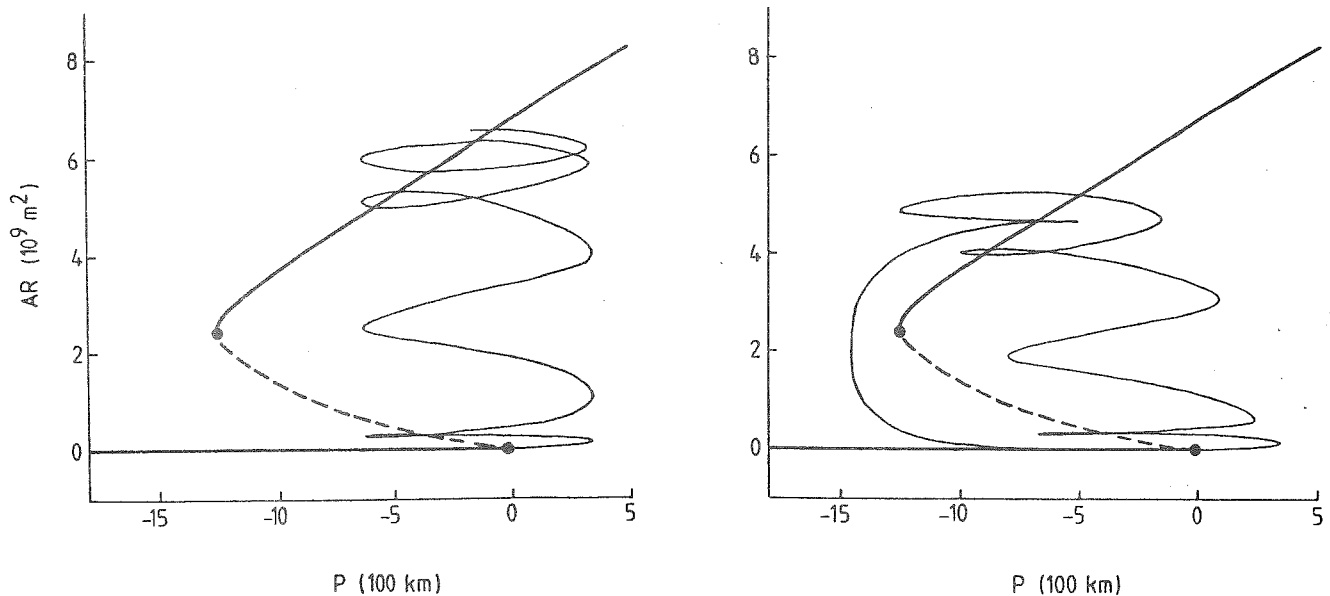
Let us assess the importance of bedrock sinking by scaling. If an ice sheet grows to an equilibrium state (i.e. the equilibrium state without bedrock adjustment) in which it has an average thickness of about 3000 m, the average bedrock depression required to obtain isostatic equilibrium is about 1000 m. To a first approximation, this is equivalent to raising the equilibrium line by 1000 m. If the equilibrium line has a slope of 0.0006, this corresponds to a poleward shift of the climate point over roughly 1600 km. It is obvious that this, together with a shift due to a maximum of insolation, may bring the climate point north of the critical point in the hysteresis diagram (Figs. 18 and 19).

Of course there are complications. Bedrock sinking will be largest near the centre of the ice sheet and the bedrock will thus have a considerable slope, affecting the profile of the ice sheet. The sheet will become thicker which partly cancels the effective increase of the height of the equilibrium line. This does not essentially change the mechanism, however.

To illustrate the explanation of a glacial cycle outlined above, let us consider trajectories of the ice sheet in an ice-sheet size/ climate point diagram (Fig. 29). The left panel applies to the case without bedrock sinking and corresponds to the first run shown in Fig. 28. The approach to the stationary oscillation around some equilibrium state is clearly seen. For the sake of clarity, the trajectory is drawn until $t=90$ ka. Since $dAR/dt > 0$ in the wedge of the solution diagram, and $dAR/dt < 0$ elsewhere, the trajectory indicates where the equilibrium solutions are located. With the knowledge obtained in sections 4.2 and 4.3 the solution diagram shown has simply been sketched in and was not computed separately for the model version used. It differs from that of Fig. 19 mainly because of a different value for \mathcal{X} (the slope of the equilibrium line).

If bedrock sinking is included, this may be represented by shifting P to the left. In doing so, some ambiguity cannot be

Fig. 29. Trajectories of the ice sheet for the case without bedrock sinking (left) and with bedrock sinking (right). Extremes of the trajectories with regard to P are separated by 10 ka (the period of forcing is 20 ka). Heavily drawn lines indicate equilibrium solutions (solid=stable; dashed=unstable).



avoided because we don't know exactly how the bedrock sinking can be represented by a change in P. In the second panel of Fig. 29, P moves northward over a distance of 1000 km during the ice-sheet evolution, first very slowly and then more rapidly due to the increased thickness of the sheet. The trajectory shown corresponds to the second run displayed in Fig. 28. It appears that the slower growth and the subsequent rapid decay of the ice sheet agrees with the solution diagram. From the figure we see that the complete disappearance of the ice sheet is in fact possible because of the high melting rates. If melting would be small, the trajectory could easily come into the wedge of the solution diagram again: it could cross the unstable limit line, dashed in the figure, just below the critical point. Altogether, it is the combination of lagging bedrock sinking and asymmetric mass balance (melting rates can be much larger than accumulation rates) that creates an asymmetric glacial cycle with

a time scale much larger than that of the forcing.

Finally, we note that two conditions should be fulfilled before another glacial cycle may start:

- (i) the bedrock has to be raised again,
- (ii) a summer insolation minimum of sufficient strength and duration should occur.

7.4 Simulation of the global ice-volume record

In view of the previous results, the reader may imagine that it was very tempting to integrate the ice-sheet model while forcing it with the Milankovitch radiation variations, according to section 6.5.

Fig. 30 shows results of the first two runs carried out. The only difference between those two runs is the point in time at which the integration is started (t_0), $t_0 = 750$ ka BP and $t_0 = 700$ ka BP respectively. The parameter set used is: $Z = 1.65$ m/yr, $G_{lim} = 0.5$ m/yr, $\chi = 0.0007$, $\theta^* = 30$ ka.

Although the character of the simulated curves is similar, the correlation between the curves appears to be very small. Here we face a serious problem: the model results are very sensitive to t_0 . Other runs, not shown here, revealed a similar sensitivity to the initial

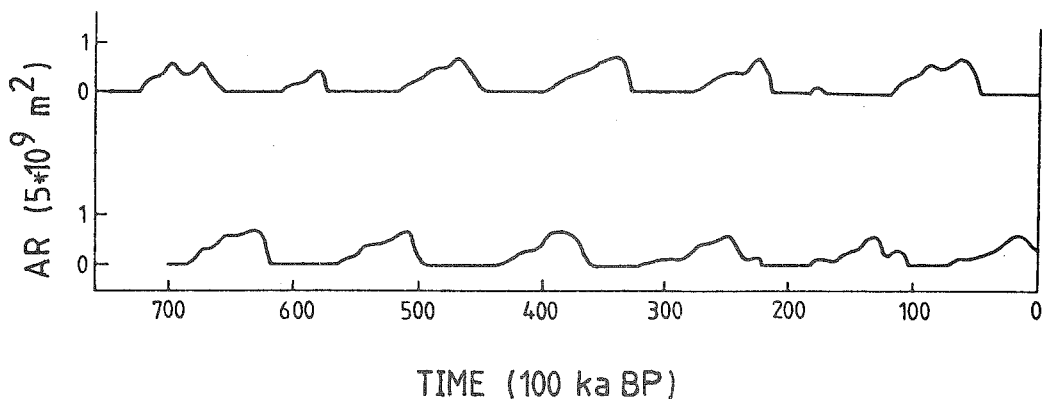


Fig. 30. Two runs with the ice-sheet model in which the Milankovitch radiation variations are imposed. The only difference between the runs is the point in time at which the integration is started. Model parameters are given in the text.

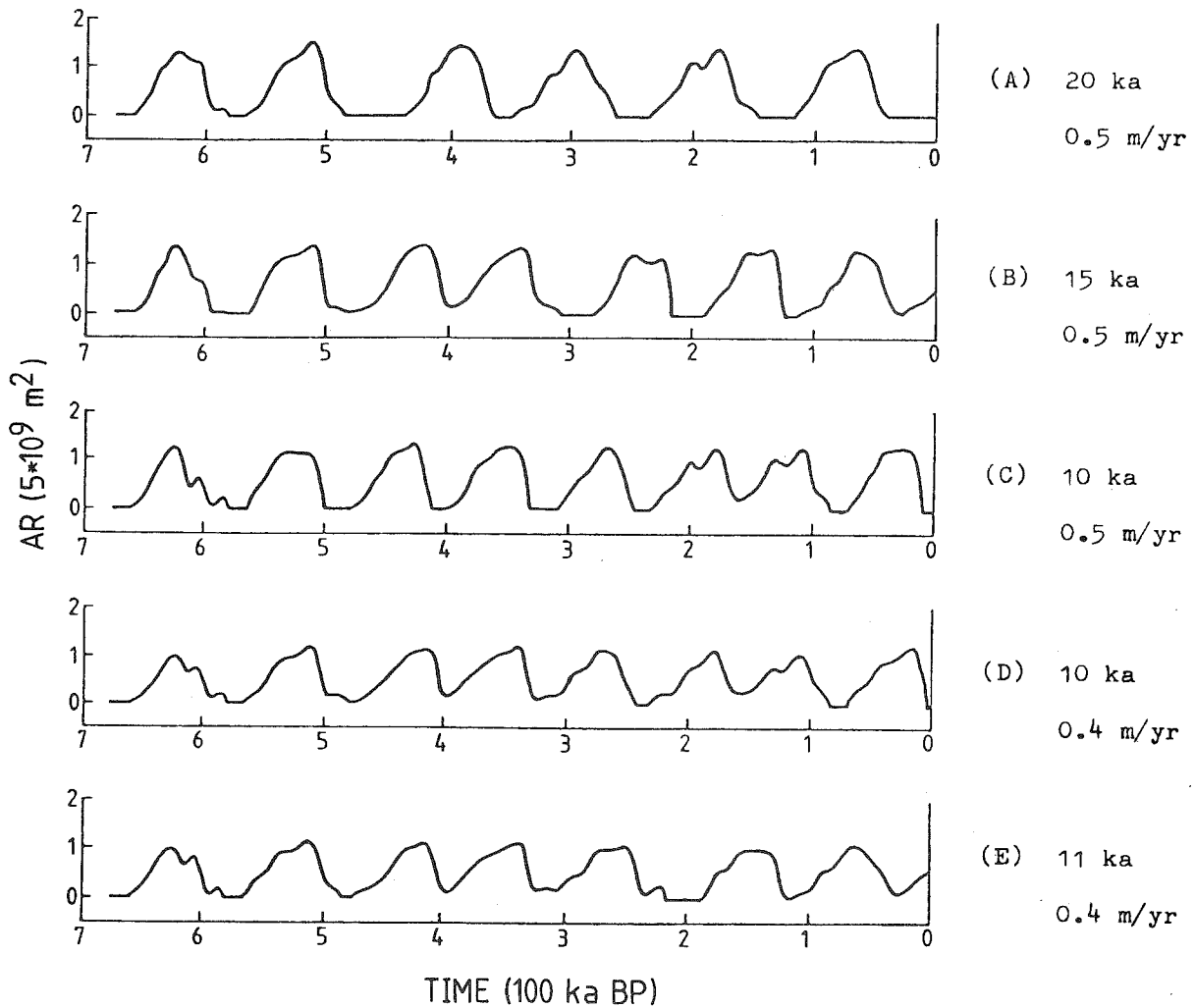
conditions. The runs shown in Fig. 30 use as initial condition $H(x)=0$ and $\xi(x)=0$, but we cannot be sure that this is a proper way to start the model. We have to accept this uncertainty, however.

The curves displayed in Fig. 30 have some shortcomings: only six glacial cycles are reproduced in the last 700 ka while the oxygen isotope record (Fig. 1) suggests a number of seven or eight, the interglacials are too long, and the amplitude of the glacial cycles is too small. Since the uncertainty in the model parameters is rather large, it makes sense to adjust these parameters in such a way that a better simulation of the ice-volume record is obtained. This also gives an impression of how sensitive the results of the model are to variations in the model parameters.

After having carried out a large number of runs it was found that the only realistic way to obtain a maximum ice-sheet size of about 2500 km is to decrease the parameter χ (slope of the equilibrium line) or to decrease the flow constant K (see eq. (25)). These parameter changes effectively enhance the strength of the surface elevation - mass balance feedback (compare this to the results in section 4.2, where χ/σ appears to be the relevant parameter). In the model runs to be discussed now, the value of χ has been decreased to 0.00045, whereas the flow constant was not changed. In addition, the value of Z (which determines the 'glaciation threshold'), was decreased from 1.65 to 1.5 m/yr. Fig. 31 shows five model runs with this model version. Results are shown for five different combinations of the parameter set G_{lim}, θ^* .

The first three runs only differ in the value for θ^* . Apparently, if the value of θ^* decreases, the number of glacial cycles in the 675 ka time span increases. This effect is not very strong, however. Doubling θ^* from 10 ka (run C) to 20 ka (run A) results in the transition from an eight-cycle regime to a six-cycle regime. Run C is particularly interesting because the last termination produced by the model (about 10 ka BP) is in excellent agreement with the proxy data record. The very rapid decrease of the ice volume, known from all kinds of geological evidence, comes out sharply. However, the simulated last glacial cycle seems to be shorter than the one occurring in the oxygen isotope record. Therefore, the simulated record may be out of phase with reality most of the time.

Fig. 31. Model integrations for the last 675 ka, with $Z=1.5$ m/yr and $\chi=0.00045$. The runs differ with regard to the values of the parameters G_{lim} and θ^* ; these values are given on the right-hand side of each curve. In all integrations, initial conditions were $H(x)=\zeta(x)=0$ at $t_0=675$ ka BP. In terms of meridional ice-sheet size, one unit on the vertical axis corresponds to a size of approximately 2000 km.



In run D the upper limit to the mass balance (G_{lim}) was decreased from 0.5 to 0.4 m/yr. The effect is rather small, although the asymmetric shape of the glacial cycles becomes somewhat more pronounced.

Run E is similar to run D except that a small change was made in the value of θ^* . The resulting modification of the ice-volume curve is not small, however! Curves E and D start to diverge at $t=230$ ka BP. Apparently, in run E the bedrock raises so slowly that the insolation maximum at 220 ka BP cannot be survived by the small ice sheet that was initiated at 230 ka BP. This brings run E completely out of phase with run D.

The type of behaviour described above appeared to be typical for variations in most model parameters or slight changes in initial conditions. The major conclusion of the sensitivity experiments carried out is that the character of the simulated ice-volume curves (asymmetry of the glacial cycle, 100 ka period) is rather insensitive to changes in the model parameters, whereas the phase of the glacial cycles is very sensitive to such changes. It is very well possible that this model behaviour reflects a realistic feature. To visualize this point, it means for example that if ten globes, differing only very slightly from each other, go through the same insolation variations, the resulting ice-volume records may differ considerably in timing, but show the same type of glacial cycle. Or, in other words, the system exhibits a stochastic-periodic behaviour.

The model simulations strongly suggest that the 100 ka glacial cycle is mainly internally generated, and not directly forced by insolation variations on this time scale. A statistical study of Komiz and Pisias (1979) supports this view: they show that in coherence spectra of an oxygen isotope record (which was first dated as accurately as possible) and the orbital parameters no significant peak is found around a period of 100 ka.

8. DISCUSSION

The 'complete climate model', requiring moderate computational resources, has not yet been constructed. As illustrated by the contents of this thesis, one is therefore forced to study components of the climate system separately. Here, the ice-albedo-temperature feedback and the surface elevation-mass balance feedback have been studied in some detail, but no proof is given that these processes are indeed most important with regard to climate sensitivity. To illustrate the ambiguity involved: ice-age theories have been proposed in which long-term changes in the oceanic circulation drive the glacial cycles.

In spite of the fact that in the climate system no single process works in an isolated way, it makes sense to isolate such a process for detailed investigations. This may give considerable insight, and it is worthwhile to know how far one can get in explaining climatic variations by ruling out all other processes. This is in fact what has been done in this study. It has led to the conclusion that the ice-albedo-temperature loop constitutes a rather weak positive feedback in the climate system. In contrast, the coupling between the surface elevation and mass balance of an ice sheet appeared to be very important in enhancing climate sensitivity. Let us consider these main conclusions in somewhat more detail.

Experiments with the energy-balance climate model, in which the solar constant was slightly changed, showed that the sensitivity of the surface temperature to insolation variations was too small to explain the pleistocene climatic variations from changes in the orbital parameters of the earth. This is a direct consequence of the important role that cloud cover plays in determining the planetary albedo. Since in the model cloud cover is fixed, changes in the albedo due to changes in surface conditions (snow and ice cover) are limited. This is a weak point in this (and most other) climate model(s). The internal freedom of the climate model is further decreased by keeping the energy-transport coefficients constant (apart from the effect of sea ice), and by neglecting the effect of the yearly cycle. It is obvious, however, that in reality cloud

cover, oceanic and atmospheric circulation, and the yearly cycle will change if the forcing of the climate system changes. For example, an increased albedo difference between oceanic and continental regions will cause a larger temperature difference between those regions, to which the atmospheric circulation will react. We may imagine that the atmospheric circulation becomes less zonal, which implies that the energy exchange between ocean and continent will be reduced. This process enhances the ocean-continent temperature difference. The potential importance of such a process can be studied by varying the appropriate transport coefficient in the model (see section 3.2), but the real importance cannot be assessed because it is unknown how the transport coefficients change if the temperature distribution changes.

In view of these points, the results of the experiments with the climate model should be considered as order-of-magnitude estimates. But even then we cannot escape the feeling that the ice-albedo-temperature feedback is too weak to explain the pleistocene climatic variations. A consequence of this conclusion is that Wilson's (1964) ice-age theory cannot be supported. This theory, which has become rather popular, tells that a glacial starts after surging of a part of the Antarctic Ice Sheet. The enormous mass of ice sliding into the sea would form an ice shelf covering the southern oceans south of about 50°S . The associated increase in planetary albedo would cause the global surface temperature to drop to a level at which glaciation in the Northern Hemisphere starts. This process would occur every 100 ka (the time needed to build up the West-Antarctic Ice Sheet again). According to the present model results, the increase of the planetary albedo due to the presence of an ice shelf would be very small, particularly because in the latitude belt involved cloud cover is very large (over 70 %; e.g. Berliand and Strokina, 1975). But even if during such an event cloud cover would decrease substantially, the planetary albedo would hardly be effected because at the latitudes involved the cloud albedo is almost as high as the clear-sky albedo over an ice surface. Anyway, the climate model developed in this thesis predicts a drop in global temperature of about 0.5 K if such an ice shelf occurs. This seems to be too small to control glaciation on the Northern Hemisphere continents.

The study of the height-mass balance feedback has led to more spectacular results. The Northern Hemisphere ice-sheet model is able to produce ice-volume records that resemble 'observed' records in character. It is therefore tempting to state that the pleistocene glacial cycles may be explained completely by the nature of the ice sheet/bedrock dynamics. However, ice-sheet modelling also has its problems and uncertainties, and it seems wiser to suggest rather than to state that ice sheet/bedrock dynamics are most important in creating the 100 ka glacial cycle.

In ice-sheet model studies of the present kind, the major problem is the parameterization of the mass balance. In particular accumulation is difficult to handle. A growing ice sheet will certainly affect the atmospheric circulation around it, which in turn influences the accumulation pattern. Orographically forced precipitation may be very important, and may form an effective feedback loop.

The ice-sheet model used in chapter 7 assumes a bedrock that is originally flat. Experiments not shown here (but discussed in ref.[6]) indicate that the behaviour of an ice sheet may change if mountain ranges are present. This is an important point for further study.

Another shortcoming in the model employed is the fact that the flow constant K is not allowed to vary. In reality, a large ice sheet will gradually become warmer due to the geothermal heat flux at its base and due to mechanical dissipation. If ice is warmer it flows easier, and this should be reflected in the ice-sheet model by an increase of K . It is even possible that the temperature at the base of the ice sheet reaches the melting point, which may set in motion surging of the ice sheet. This could provide an alternative explanation for the instability occurring if an ice sheet is full-grown. In the present study such effects has not been dealt with, but it is obvious that these points deserve to be studied.

Reviews of ice-age theories usually center around the question 'Is the Milankovitch theory correct?'. To preserve historical continuity, let us try to answer this question on the basis of the material presented in this thesis. First of all, the results of chapter 7 show that the 100 ka glacial cycle, which dominates the paleoclimatic record, is internally generated. It is not forced

by variations in insolation on the 100 ka time scale (mainly due to changes in the eccentricity of the earth's orbit). Internally generated here means that the character of the model output depends more on intrinsic properties of the climate system than on the shape of the input (i.e. the spectrum of the insolation variations). The relevant intrinsic properties are the asymmetry in the mass balance (melting rates can be much higher than accumulation rates), and the fact that bedrock sinking occurs and lags ice-sheet size. However, to produce a 100 ka periodicity the model needs to be driven by insolation variations, for example by the Milankovitch insolation variations. If the forcing is kept constant in time, the model ice-sheet tends towards a steady state (a large ice sheet or no ice sheet at all, depending on the forcing and the initial conditions). If the model would be forced by white noise of sufficient strength, an ice-volume record would show up in which an asymmetric 100 ka cycle appears again. So all kinds of insolation variations (dust veils, changes in solar activity) may generate glacial cycles, but it may very well be that only the Milankovitch variations are of sufficient strength. In this view, the Milankovitch hypothesis could be considered correct. On the other hand, earlier versions of the Milankovitch theory (including his own view) assume that the global ice volume is proportional to insolation averaged over some latitude belt and over some part of the year (mostly summer). In later versions, the rate of growth (or decay) was set proportional to insolation. The present results clearly demonstrate that such assumptions are not correct. In the model integrations presented in chapter 7, the ice sheet sometimes grows in a period of high insolation, and sometimes decays if insolation is below normal. This leads to the conclusion that the Milankovitch theory, in which a linear relationship between ice-sheet size (growth) is a crucial link, must be rejected in view of the present model results.

In this work no attention has been paid to the problem of ice-age initiation. In the model experiments a suitable glaciation threshold was incorporated by giving the model parameter Z such a value that an insolation minimum initiates an ice sheet. This ambiguity cannot be avoided, but it raises questions. How does a

glacial start ?, and where ? It is unlikely that the American and Eurasian Ice Sheets are always completely in phase. At present, Scandinavia seems to be the most favourable place for an ice sheet to develop. Here, a 600 m lowering of the equilibrium plane seems to be enough to start the growth of a large ice sheet (ref. [7]). In Northeast-Canada the critical lowering seems to be well over 1000 m (L.D. Williams, unpublished manuscript). It therefore seems likely that glaciation starts in Scandinavia. A point of considerable interest is whether the climate system permits a state in which only one of the sheets mentioned above is present. To answer this type of questions, more advanced modelling is necessary. The ice-sheet model developed in this study could be used as a basis to construct separate models for the Eurasian and Laurentide Ice Sheets in which orography is taken into account, and which could be coupled to a prescribed degree.

Where models are integrated in time, they can be integrated into the future. So in studies of the present type, one usually encounters a prediction of the future climate. On the basis of the results presented in chapter 7, a few inferences on this topic can be made.

We can be rather sure that in the future a new glacial will start, and that it will come to an end again. In view of the fact that the climate system seems to behave in a stochastic-periodic way it is difficult to say when glaciation will start. In the ice-sheet model, the point in time at which an ice sheet is initiated depends strongly on the precise values of Z (the glaciation threshold), θ^* (time scale for bedrock adjustment), etc. From this we may conclude that for example the CO_2 warming (due to burning of fossil fuel) may shift the point where a new glacial starts forward in time, but once the glacial is initiated the 100 ka cycle will be completed.

Of course, the probability of ice-age initiation will be larger if insolation is lower. However, in the forthcoming 100 ka the summer insolation minima at high latitudes will be comparatively weak and probably close to the glaciation threshold. The present interglacial could therefore last longer than was usual during the last 700 ka.

REFERENCES

A. Articles on which this thesis is based (referred to in the text by means of square brackets).

1. J. Oerlemans and H.M. van den Dool (1978): Energy balance climate models: stability experiments with a refined albedo and updated coefficients for infrared emission. J. Atmos. Sci. 35, 371-381.
2. J. Oerlemans (1980): On zonal asymmetry and climate sensitivity. Tellus, in press.
3. ——— (1980): Continental ice sheets and the planetary radiation budget. Quaternary Res., in press.
4. ——— and J.M. Bienfait (1980): Linking ice sheet evolution to Milankovitch radiation variations: a model simulation of the global ice volume record. In: Proceedings of the Sun and Climate conference, CNES/CNRS, Toulouse, 30 Sept. - 3 Oct. 1980.
5. J. Oerlemans (1980): On the stability of Northern Hemisphere continental ice sheets. KNMI Scientific Rep. WR 80-2, 13 pp.
6. ——— (1980): Some basic experiments with a vertically-integrated ice sheet model. Tellus, in press.
7. ——— (1980): Modelling Pleistocene European ice sheets: experiments with simple mass-balance parameterizations. Quaternary Res., in press.
8. ——— (1979): A model of a stochastically driven ice sheet with planetary wave feedback. Tellus 31, 469-477.

B. General references.

- Andrews, J.T., and M.A.W. Mahaffy (1976): Growth rate of the Laurentide Ice Sheet and sea level lowering (with emphasis on the 115 000 BP sea level low). Quaternary Res. 6, 167-183.
- Berger, A.L. (1978): Long-term variations of daily insolation and quaternary climatic changes. J. Atmos. Sci. 35, 2362-2367.
- (1980): Milankovitch astronomical theory of paleoclimates, a modern review. Vistas in Astronomy, in press.
- Berliand, T.G., and L.A. Strokinina (1975): Cloud regime over the globe. In: Proceedings of GGO, Physical Climatology, No. 338, Leningrad.
- Bodvarsson, G. (1955): On the flow of ice sheets and glaciers. Jökull 5, 1-8.
- Budd, W.F., and B. McInnes (1975): Modelling of periodically surging glaciers. Science 186, 925-927.
- Budyko, M.I. (1969): The effect of solar radiation variations on the climate of the earth. Tellus 21, 611-619.
- Calder, N. (1974): Arithmetic of ice ages. Nature 252, 216-218.
- Cess, R.D. (1976): Climatic change: an appraisal of atmospheric feedback mechanisms employing zonal climatology. J. Atmos. Sci. 33, 1831-1843.
- Charlesworth, J.K. (1957): The quaternary era. Edward Arnold Ltd., London.
- Chorlton, J.C. and H. Lister (1968): Snow accumulation over Antarctica. In: ISAGE-proceedings, Int. Ass. Scient. Hydrol. Pub 86, 254-263.
- CLIMAP (1976): The surface of the ice-age earth. Science 191, 1131-1137.
- Coakley, J.A. (1979): A study of climate sensitivity using a simple energy balance model. J. Atmos. Sci. 36, 260-269.
- and B.A. Wielicki (1979): Testing energy balance climate models. J. Atmos. Sci. 36, 2031-2039.
- Dool, H.M. van den (1980): On the role of cloud amount in an energy-balance model of the earth's climate. J. Atmos. Sci. 37, 939-946.
- Ellis, J.S., and T.H. Vonder Haar (1976): Zonal average earth radiation budget measurements from satellites for climate studies. Atmos. Sci. Paper No. 240, Colorado State University.

- Flint, R.F. (1971): Glacial and quaternary geology. Wiley, New York.
- Frankignoul, C., and K. Hasselmann (1977): Stochastic climate models, part 2, application to sea-surface temperature anomalies and thermocline variability. Tellus 29, 289-305.
- Gal-Chen, T., and S.H. Schneider (1976): Energy balance climate modeling: comparison of radiative and dynamic feedback mechanisms. Tellus 28, 108-121.
- Hasselmann, K. (1976): Stochastic climate models, part 1, theory. Tellus 28, 473-485.
- Hays, J.D., J. Imbrie and N.J. Shackleton (1976): Variations in the earth's orbit: pacemaker of the ice ages. Science 194, 1121-1132.
- Heath, G.R. (1979): Simulations of a glacial paleoclimate by three different atmospheric general circulation models. Palaeogeography, Palaeoclimatology, Palaeoecology 26, 291-303.
- Held, I.M., and M.J. Suarez (1974): Simple albedo feedback models of the ice caps. Tellus 26, 613-629.
- Heuvel, E.P.J. van den (1966): On the precession as a cause of Pleistocene variations of Atlantic ocean water temperatures. Geophys. J. Astr. Soc. 11, 323-336.
- Hollin, J.T. (1972): Interglacial climates and Antarctic ice surges. Quaternary Res. 2, 401-408.
- Imbrie, J., J. van Donk and N.G. Kipp (1973): Paleoclimatic investigation of a late pleistocene Caribbean deep-sea core: comparison of isotopic and faunal methods. Quaternary Res. 3, 10-38.
- and K.P. Imbrie (1979): Ice ages: solving the mystery. MacMillan Press Ltd., London.
- and J.Z. Imbrie (1980): Modeling the climatic response to orbital variations. Science 207, 943-953.
- Källen, E., C. Crafoord and M. Ghil (1979): Free oscillations in a climate model with ice-sheet dynamics. J. Atmos. Sci. 36, 2292-2303.
- Kominz, M.A., and N.G. Pisias (1979): Pleistocene climate: deterministic or stochastic? Science 204, 171-173.
- Laevastu, T. (1960): Factors affecting the temperature of the surface layer of the sea. Soc. Sci. Fennica Commentations, Physical Mathematics 25.
- Lemke, P. (1977): Stochastic climate models, part 3, application to zonally averaged energy models. Tellus 29, 385-392.

- Lian, M.S., and R.D. Cess (1977): Energy balance climate models: a reappraisal of ice-albedo feedback. J. Atmos. Sci. 34, 1058-1062.
- Lindzen, R.S., and B. Farrell (1977): Some realistic modifications of simple climate models. J. Atmos. Sci. 34, 1487-1501.
- Lumb, F.E. (1964): The influence of cloud on hourly amounts of total solar radiation at the sea surface. Quart. J. Roy. Met. Soc. 90, 43-56,
- Manabe, S., and R. Wetherald (1967): Thermal equilibrium of the atmosphere with a given distribution of relative humidity. J. Atmos. Sci. 24, 241-259.
- and D.C. Hahn (1977): Simulation of the tropical climate of an ice age. J. Geophys. Res. 82, 3889-3912.
- North, G.R. (1975): Theory of energy-balance climate models. J. Atmos. Sci. 32, 2033-2043.
- Nye, J.F. (1959): The motion of ice sheets and glaciers. J. Glaciol. 3, 493-507.
- Oort, A.H. (1980): Global Atmospheric Circulation Statistics, 1958-1973. NOAA Professional Paper, U.S. Government Printing Office, Washington D.C., in press.
- (1977): The interannual variability of atmospheric circulation statistics. NOAA Professional Paper No. 8, U.S. Government Printing Office, Washington D.C.
- and E.M. Rasmusson (1971): Atmospheric circulation statistics. NOAA Professional Paper No. 5, U.S. Government Printing Office, Washington D.C.
- Paterson, W.S.B. (1969): The physics of glaciers. Pergamon Press, Oxford.
- Pittock, A.B., L.A. Frakes, D. Janssen, J.A. Peterson and J.W. Zillman (1978): Climatic change and variability. Cambridge University Press, Cambridge.
- Pollard, D. (1978): An investigation of the astronomical theory of the ice ages using a simple climate-ice sheet model. Nature 272, 233-235.
- Raschke, E., T.H. Vonder Haar, W.R. Bandeen and M. Pasternak (1973): The annual radiation balance of the earth-atmosphere system during 1969-1970 from Nimbus-3 measurements. J. Atmos. Sci. 30, 341-264.

- Schneider, S.H., and T. Gal-Chen (1973): Numerical experiments in climate stability. J. Geophys. Res. 78, 6182-6194.
- Sellers, W.D. (1969): A global climatic model based on the energy balance of the earth-atmosphere system. J. Applied Meteorol. 8, 392-400.
- (1974): Climate models and variations in the solar constant. Geofysica Internacional 14, 303-315.
- Shackleton, N.G. and N.D. Opdyke (1973): Oxygen isotope and paleomagnetic stratigraphy of Equatorial Pacific core V28-238: oxygen isotope temperatures and ice volumes on a 10^5 and 10^6 year scale. Quaternary Res. 3, 39-55.
- and ——— (1976): Oxygen isotope and paleomagnetic stratigraphy of Pacific core V28-239, late Pliocene to latest Pleistocene. Geol. Soc. Am. Mem. 145, 449-464.
- Sugden, D.E., and B.S. John (1976): Glaciers and Landscape. Edward Arnold Ltd., London.
- Turcotte, D.L. (1979): Flexure. In: Advances in Geophysics (Ed.: B. Saltzman, Academic Press, New York), 51-86.
- Weertman, J. (1961): Stability of ice-age ice sheets. J. Geophys. Res. 66, 3783-3792.
- (1976): Milankovitch solar radiation variations and ice age ice sheet sizes. Nature 261, 17-20.
- Wetherald, R., and S. Manabe (1975): The effects of changing the solar constant on the climate of a general circulation model. J. Atmos. Sci. 32, 2044-2059.
- Wilson, A.T. (1964): Origin of ice ages: an ice shelf theory for Pleistocene glaciation. Nature 201, 147-149.

CURRICULUM VITAE

Johannes Oerlemans werd op 8 oktober 1950 geboren te Eethen (Noord-Brabant). Na het doorlopen van de lagere school bezocht hij de Rijks-HBS te Bergen op Zoom; het diploma werd behaald in 1969. In dat jaar begon hij met de studie natuurkunde (richting N3) aan de Rijksuniversiteit te Utrecht.

Het kandidaatsexamen werd behaald in 1972, het doktoraal examen (cum laude) in 1976. Het doktoraalpakket bestond uit het hoofdvak meteorologie en de bijvakken toegepaste wiskunde en fysische oceanografie.

Van 16 Oktober 1976 tot 1 september 1980 was de auteur werkzaam bij het KNMI te De Bilt, in de werkgroep 'Algemene cirkulatie en klimaatschommelingen' van de afdeling Meteorologisch Onderzoek. In deze periode werkte hij gedurende enkele maanden op het 'National Center for Atmospheric Research' te Boulder (USA).

Sinds 1 september 1980 is J. Oerlemans in dienst bij de Rijksuniversiteit te Utrecht. Hij is als wetenschappelijk medewerker verbonden aan het Instituut voor Meteorologie en Oceanografie.

Huidig adres:

J. Oerlemans
Instituut voor Meteorologie en Oceanografie
Princetonplein 5
Utrecht

